

SCIENTIFIC REPORTS



OPEN

Sugar based *N,N'*-didodecyl-*N,N'*-digluconamideethylenediamine gemini surfactant as corrosion inhibitor for mild steel in 3.5% NaCl solution-effect of synergistic KI additive

Ruby Aslam¹, Mohammad Mobin¹, Jeenat Aslam¹ & Hassane Lgaz^{2,3}

The inhibitory behaviour of non-ionic sugar based *N,N'*-didodecyl-*N,N'*-digluconamideethylenediamine gemini surfactant, designated as Glu(12)-2-Glu(12) on mild steel (MS) corrosion in 3.5% NaCl at 30–60 °C was explored using weight loss, PDP, EIS and SEM/EDAX/AFM techniques. The compound inhibited the corrosion of mild steel in 3.5% NaCl and the extent of inhibition was dependent on concentration and temperature. The inhibiting action of Glu(12)-2-Glu(12) is synergistically enhanced on addition of potassium iodide (KI) at all concentrations and temperatures. The inhibiting formulation comprising of 2.5×10^{-3} mM of Glu(12)-2-Glu(12) and 10 mM of KI exhibits an inhibition efficiency of 96.9% at 60 °C. Quantum chemical calculations and MD simulation were applied to analyze the experimental data and elucidate the adsorption behaviour and inhibition mechanism of inhibitors. MD simulation showed a nearly parallel or flat disposition for Glu(12)-2-Glu(12) molecules on the MS surface providing larger blocking area to prevent the metal surface from corrosion.

The significance of mild steel cannot be undervalued in the constructions and chemical industries based on their cost effectiveness, obtainability and immense mechanical properties. However, the poor corrosion resistance of mild steel limits its application^{1–3}. One of the methods to efficiently control corrosion processes is the employment of corrosion inhibitors.

Several researchers have dealt with the synthesis and investigation of surfactants (cationic, anionic, non-ionic and zwitterionic) as corrosion inhibitors in various medium^{4–9}. Non-ionic surfactants, which have no apparent charge on the head group, have notably lower critical micelle concentrations (CMCs) in comparison to the analogous ionic surfactants and are reported to possess high inhibition efficiencies for corrosion of metals in chloride media^{10,11}. A novel class of surfactants called gemini, which consists of two hydrophobic chains and two polar/ionic head-groups united covalently by a rigid or flexible spacer has emerged during the last few years. When equated with single-head, single tail counterparts, these gemini surfactants offer better surface properties like much smaller CMC values, much greater efficiency in reducing surface tension than expected^{12–14} etc. Due to their greater performance, geminis have been generating increasing interest among researchers.

The surfactants as well as majority of the other inhibitors frequently employed in the industries are composed of some compounds that are unsafe and have been presently facing a lot of criticisms due to their threat to human and their environments. In the past two decade, the research in the field of 'green' corrosion inhibitors

¹Corrosion Research Laboratory, Department of Applied Chemistry, Faculty of Engineering and Technology, Aligarh Muslim University, Aligarh, 202002, India. ²Laboratory of Applied Chemistry and Environment, ENSA, Ibn Zohr University, PO Box 1136, 80000, Agadir, Morocco. ³Department of Applied Bioscience, College of Life & Environment Science, Konkuk University, 120 Neungdong-ro, Gwangjin-gu, Seoul, 05029, South Korea. Correspondence and requests for materials should be addressed to M.M. (email: drmmobin@hotmail.com)

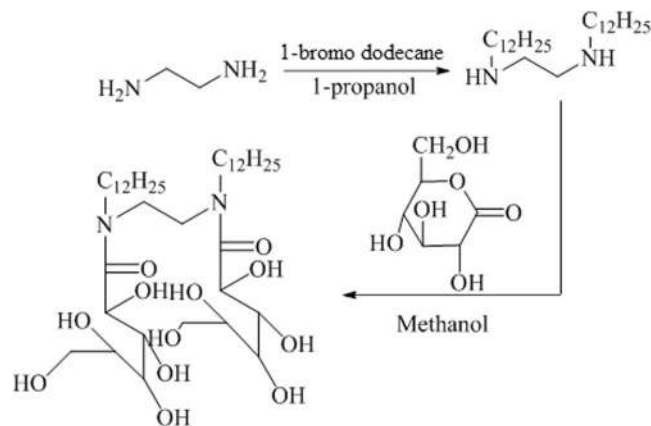


Figure 1. Pathway for the synthesis of Glu(12)-2-Glu(12) gemini surfactant.

has been aimed toward the goal of using affordable, potent molecules with little or “zero” negative environmental impact^{15,16}.

In view of the absence of toxicity, very good bio-degradability and dermatological compatibility, the use and production (industrial scale) of sugar-based surfactants has gradually increased in the recent past¹⁷. Furthermore, these surfactants also offer unexplored possibilities in the development of synthetic bio-molecules with unique and novel surface active properties.

One potential method to cost-effectively increase the corrosion inhibition efficiency is to employ the concept of synergism and utilize a combination of inhibitors^{18,19}. The phenomenon of synergism in corrosion inhibition signifies the enhancement in the ability of an inhibitor to resist corrosion in the presence of secondary species in the corrosive medium. Halide ions are effective additives for surfactants in corrosion inhibition of steel in different media^{20–24}.

In this paper, we are reporting the preparation of a sugar based non-ionic gemini surfactant, *N,N'*-didodecyl-*N,N'*-digluconamidediethylenediamine, designated as Glu(12)-2-Glu(12). After confirming the structure of this sugar based non-ionic gemini surfactant, we evaluated its surface activities. A perusal of literature on corrosion inhibitors suggest that there is no published report on the corrosion inhibition effect of Glu(12)-2-Glu(12). Therefore, the present study was undertaken to assess the corrosion inhibition effect of, Glu(12)-2-Glu(12) gemini surfactant for mild steel in 3.5% NaCl solution using chemical and electrochemical techniques. Effect of electrolyte temperature (temperature range 30–60 °C) on corrosion inhibition of Glu(12)-2-Glu(12) has also been assessed and discussed. The associated activation energy of corrosion, enthalpy of activation, entropy of activation, and thermodynamic parameters such as equilibrium constant, standard free energy of adsorption, and entropy of adsorption were computed to elaborate the corrosion inhibition mechanism. Synergistic inhibition between Glu(12)-2-Glu(12) gemini surfactant and potassium iodide (KI) in 3.5% NaCl solution has also been investigated by means of weight loss and electrochemical methods, and the possible synergistic mechanism has been proposed. DFT calculations and MD simulation was employed in an attempt to understand the adsorption of Glu(12)-2-Glu(12) molecules on mild steel surface at the molecular level.

Materials and Methods

Materials and measurements. The tested material was commercially obtained mild steel, with the chemical composition (wt %), as analysed by optical emission spectrometer, was as follows: C-0.061, Mn-0.181, P-0.018, Cr-0.035, Mo-0.054, Al-0.017, V-0.034 and Fe-99.59. The mild steel was cut into 2.5 cm × 2 cm × 0.1 cm samples for weight loss measurements. For electrochemical measurements, circular specimens, with exposed surface area 1.0 cm², were used. Then the samples were grated with 320#, 400#, 600# and 1200# abrasive papers in turn, rinsed with double distilled water and degreased with alcohol and acetone.

Preparation of *N,N'*-didodecyl-*N,N'*-digluconamidediethylenediamine, Glu(12)-2-Glu(12). The gemini surfactant, Glu(12)-2-Glu(12), was synthesized in two steps following the procedure described in the literature²⁵. Detailed experimental procedure described for the preparation of gemini surfactant and characterization are given as follows.

Figure 1 shows the synthetic route of gemini surfactant. In the first step *N,N'*-dialkyldiethylenediamine was prepared by the reaction of ethylenediamine with 1-propanol and 1-bromododecane (added drop wise) under a mild alkaline condition with methanolic NaOH solution. The mixture was refluxed for 24 h. After the filtrate was evaporated, the residue was poured in an aqueous NaOH solution and was stirred for 6 h. After filtration of the obtained crystalline white product from the diethyl ether solution, re-crystallization was performed three-times using a mixed solvent of ethanol containing a little amount of methanol. In the second step D-(+)-Gluconolactone was added to a methanolic solution of *N,N'*-dialkyldiethylenediamine. The mixture was stirred for 1 week at room temperature, refluxed for 3 h and then evaporated. The obtained residue was washed with hexane three times to remove un-reacted *N,N'*-dialkyldiethylenediamine. After washing, the product was dissolved in dried acetone. Then the product was again washed with dried ethanol and finally, re-crystallized from a mixed solvent of dried acetonitrile containing a small amount of ethanol. The phlegmatic product was obtained.

The structure of the compound was confirmed by, $^1\text{H-NMR}$ and FT-IR. The data is given below.

FT-IR (KBr, cm^{-1}): 3421, 2924, 2836, 1623, 1498, 1073, 719.

$^1\text{H-NMR}$ (300 MHz, D_2O): $\delta = 0.79\text{--}0.88$ (t, 6H, $-2 \times \text{CH}_3$, alkyl chain), 1.21–1.49 (m, 36H, $-2 \times (\text{CH}_2)_9$, alkyl chain), 1.61–1.71 (m, 4H, $-2 \times \text{NCH}_2\text{CH}_2^-$), 3.275 (s, 12H, $-2 \times \text{N}^+(\text{CH}_3)_2$), 3.81 (s, 4H, $-2 \times \text{CH}_2\text{O}$), 4.31 (s, 4H, $-2 \times \text{N}^+\text{CH}_2$), 4.53 (s, 4H, $-2 \times \text{N}^+\text{CH}_2\text{COO}$).

Surface tension measurement. Surface tension measurements were performed using a SD Hardson-Kolkata tensiometer by the ring detachment method. Prior to each experiment the instrument was calibrated at 30 °C with double distilled water. Requisite concentrations of Glu(12)-2-Glu(12) alone and in combination with 10 mM KI were obtained and after complete equilibration of solutions the readings were recorded. Force engaged in the complete detachment of Pt-Ir ring from the surface film was interpreted as surface tension, γ (mN/m). Measurement of γ was continued till the equilibrium values are attained. The particular concentration at which γ vs. concentration plot shows a break approaches to the CMC.

Weight loss study. During weight loss study, the prepared mild steel specimens, were suspended in 3.5% NaCl solution in the absence and presence of different concentrations of Glu(12)-2-Glu(12) at 30, 40, 50 and 60 °C, respectively. The temperature was regulated by a thermostatic water bath. After 6 h immersion, the mild steel specimens were cleaned with a bristle brush, washed in double-distilled water and acetone, air-dried, and then reweighed.

The corrosion rate (ν , $\text{mg cm}^{-2} \text{h}^{-1}$) and inhibition efficiency (η_w %) at different concentrations were evaluated by equations (1) and (2), where W_0 and W are the weight of samples before and after immersion in 3.5% NaCl solution, respectively, A is the total surface area of the samples, t is the immersion time, ν_0 and ν are the corrosion rates in the absence and presence of the inhibitor, respectively. For weight loss measurements, triplicate experiments were performed simultaneously and the corrosion rates were averaged.

$$\nu = \frac{W_0 - W}{At} \quad (1)$$

$$\eta_w(\%) = \frac{\nu_0 - \nu}{\nu_0} \times 100 \quad (2)$$

Electrochemical measurements. The potentiodynamic polarization and electrochemical impedance (EIS) measurement tests were carried out using AUTOLAB instrument; model 128 N. A typical three electrode system from AUTOLAB was used for electrochemical tests. The system was composed of a silver/silver chloride as reference electrode, a platinum wire as counter electrode, and the mild steel sample with an exposed area of 1 cm^2 as working electrode. Before the commencement of electrochemical tests, the working electrode was immersed in the electrolytic solution for 30 min for achieving a steady state potential. The electrochemical measurements were repeated thrice under identical experimental conditions.

During polarization experiments, the potential of the working electrode was varied from cathodic to anodic direction within a range of -250 to $+250$ mV with reference to open circuit potential (OCP) at a rate of 0.001 V/s. EIS measurements was carried out in the frequency range 10^5 to 10^{-2} Hz at OCP. The sinusoidal potential perturbation was 10 mV in amplitude. The cell temperature was maintained at 30 ± 2 °C using a thermostatic water-bath.

The inhibition efficiencies (η %) were calculated by equations (3) and (4).

$$\eta_i(\%) = \frac{i_{\text{corr}} - i_{\text{corr}}^{(i)}}{i_{\text{corr}}} \times 100 \quad (3)$$

where i_{corr} and $i_{\text{corr}}^{(i)}$ is corrosion current density without and with inhibitor, respectively and η_i (%) is the inhibition efficiency obtained by potentiodynamic polarization measurement.

$$\eta_R(\%) = \frac{R_{\text{ct}}^{(i)} - R_{\text{ct}}}{R_{\text{ct}}^{(i)}} \times 100 \quad (4)$$

where R_{ct} and $R_{\text{ct}}^{(i)}$ is the charge transfer resistance without and with inhibitor, respectively and η_R (%) is the inhibition efficiency obtained by EIS measurement.

Surface characterization. In order to explore the relationship between the electrochemical behaviour and surface morphology, freshly polished mild steel coupons were suspended in 3.5% NaCl solution without and with optimum concentration of Glu(12)-2-Glu(12) for 6 h at room temperature and were examined by AFM and SEM/EDAX studies. The analysis were made using AFM-Dimension icon ScanAsyst equipped with Nanoscope V.

The SEM images were taken using a scanning electron microscope (Model: JEOL JSM- 6510LV) with EDAX attachment (Model: INCA, Oxford)

Details of operating mode of instruments and procedures for the surface analyses are reported somewhere else^{20,26–28}.

Quantum chemical calculations. DFT is a most widely accepted *ab initio* approach for modelling ground states of molecules and has been found to be successful in providing insights into the chemical reactivity and selectivity. DFT calculations were carried out using Gaussian 09 (Version D.01) program²⁹ containing correlation

inhibitor	CMC $\times 10^{-3}$ (mM)	γ_{CMC} (mN/m)	π_{CMC} (mN/m)	Γ_{max} ($10^7 \times \text{mol}/\text{m}^2$)	A_{min} ($\text{\AA}^2/\text{molecule}$)	$\Delta G_{\text{mic}}^{\circ}$ (KJ/mol)	$\Delta G_{\text{ads}}^{\circ}$ (KJ/mol)
Glu(12)-2-Glu(12)	1.3	59.34	12.46	41.40	40.10	-16.75	-17.05
Glu(12)-2-Glu(12) + KI	0.61	45.43	26.37	41.81	39.70	-18.65	-19.28

Table 1. Surface active parameters of Glu(12)-2-Glu(12) and Glu(12)-2-Glu(12) + 10 mM KI in aqueous solution.

functional of B3LYP (Lee-Yang-Paar) in addition to Becke three-parameter hybrid functional using 6-31G (d, p), 6-311G (d, p) and 6-311G++ (d, p) basis sets^{30,31}. All quantum calculations were carried out in aqueous phase using Self-Consistent Reaction Field (SCRF) theory, with Polarized Continuum Model (PCM)³². Electronic properties such as energy of the highest occupied molecular orbital (E_{HOMO}), the energy of the lowest unoccupied molecular orbital (E_{LUMO}), the energy gap, ($\Delta E = E_{\text{LUMO}} - E_{\text{HOMO}}$), ionization energy (I), electron affinity (A), electronegativity (χ), hardness (η) and fraction of electron transferred (ΔN) were calculated and recorded³³.

Molecular Dynamic (MD) Simulations

In order to model the adsorption behavior of tested inhibitor onto Fe (110) surface, MD simulations were carried out using discover module as implemented in Materials Studio 6.0 Software³⁴. Fe (110) surface was selected for the simulation of the adsorption process. A supercell with a size of $25.06 \times 25.06 \times 25.14 \text{ \AA}^3$, contains 500 H_2O and inhibitor molecule was created. This interaction simulation is performed in an area of $(25.06 \times 25.06 \times 42.73 \text{ \AA}^3)$ with periodic boundary conditions and we studied five layers of iron to ensure that the surface depth was greater than the non-cut used in the calculation. The MD simulation is performed at 30 and 60 °C under canonical play (NVT) using a time step of 1.0 fs and a simulation time of 2000 ps. The details of the simulation process can be referred to our earlier papers^{35,36}. All MD simulations were carried out with COMPASS force field³⁷. Information about the interactions between the inhibitor with Fe (110) was determined by the calculation of the interaction and binding energies using equations³⁸ (5) and (6)

$$E_{\text{interaction}} = E_{\text{total}} - (E_{\text{surface+solution}} + E_{\text{inhibitor}}) \quad (5)$$

$$E_{\text{binding}} = -E_{\text{interaction}} \quad (6)$$

where E_{total} is the total energy of the entire system $E_{\text{surface+solution}}$ referred to the total energy of Fe (110) surface and solution without the inhibitor and $E_{\text{inhibitor}}$ represent the total energy of inhibitor.

Results and Discussion

Surface active properties. Fig. S1 (supporting information) displays the surface tension (γ) of aqueous solutions of Glu(12)-2-Glu(12) as a function of concentration ($\log C$). In the low surfactant concentration the γ decreases distinctly with increasing concentration and attains a break point. The intercept of two straight lines designates the critical micelle concentration (CMC).

The surface tension data shown in Fig. S1 (supporting information) allow us to calculate some physiochemical parameters such as effectiveness (π_{CMC}), maximum surface excess (Γ_{max}), minimum surface area (A_{min}), standard free energy of micellization ($\Delta G_{\text{mic}}^{\circ}$) and standard free energy of adsorption ($\Delta G_{\text{ads}}^{\circ}$) at air/solution interface³⁹ (see Table 1).

$$\Pi_{\text{CMC}} = \gamma_{\text{water}} - \gamma_{\text{CMC}} \quad (7)$$

$$\Gamma_{\text{max}} = -\left(\frac{1}{RT}\right) \left(\frac{d\gamma}{d \ln C}\right) \quad (8)$$

$$A_{\text{min}} = \left(\frac{10^{20}}{N_A \Gamma_{\text{max}}}\right) \quad (9)$$

$$\Delta G_{\text{mic}}^{\circ} = RT \ln X_{\text{CMC}} \quad (10)$$

$$\Delta G_{\text{ads}}^{\circ} = \Delta G_{\text{mic}}^{\circ} - \Pi_{\text{CMC}}/\Gamma_{\text{max}} \quad (11)$$

where γ = surface tension in mN m^{-1} , R = gas constant ($\text{J mol}^{-1} \text{K}^{-1}$), T = absolute temperature, $(-d\gamma/d \ln C)$ = slope of the plot of γ vs. $\log C$, and N_A = Avogadro' number.

CMC of the surfactants is looked as a key factor in the determination of their effectiveness as corrosion inhibitors⁴⁰. For a surfactant to exhibit excellent corrosion inhibition, it should have a low CMC value as the effectiveness of inhibition of a surfactant decreases as the CMC value increases³⁰. On the basis of this view, Glu(12)-2-Glu(12) + KI, which shows the low CMC value, may be considered as the effective corrosion inhibitor for mild steel in corrosive 3.5% NaCl solution. On comparing data obtained for Glu(12)-2-Glu(12) with that of

Glu(12)-2-Glu(12) (mM)	KI(mM)	ν (mg cm ⁻² h ⁻¹)				η_w (%)				S_0			
		30 °C	40 °C	50 °C	60 °C	30 °C	40 °C	50 °C	60 °C	30 °C	40 °C	50 °C	60 °C
3.5% NaCl		0.056 ± 0.001	0.224 ± 0.011	0.38 ± 0.022	1.504 ± 0.088	—	—	—	—	—	—	—	—
1 × 10 ⁻⁵	—	0.041 ± 0.002	0.149 ± 0.008	0.236 ± 0.006	0.878 ± 0.044	27.1	33.5	37.9	41.6	—	—	—	—
5 × 10 ⁻⁵	—	0.035 ± 0.001	0.134 ± 0.005	0.203 ± 0.009	0.698 ± 0.029	37.4	40.2	46.6	53.6	—	—	—	—
1 × 10 ⁻⁴	—	0.029 ± 0.001	0.107 ± 0.005	0.168 ± 0.008	0.563 ± 0.033	47.9	52.7	55.7	62.7	—	—	—	—
5 × 10 ⁻⁴	—	0.024 ± 0.001	0.086 ± 0.003	0.132 ± 0.005	0.447 ± 0.022	56.5	61.7	65.4	70.3	—	—	—	—
1 × 10 ⁻³	—	0.021 ± 0.001	0.065 ± 0.003	0.096 ± 0.004	0.266 ± 0.010	63.4	71.1	74.7	82.3	—	—	—	—
1.5 × 10 ⁻³	—	0.018 ± 0.001	0.053 ± 0.001	0.079 ± 0.005	0.178 ± 0.007	67.8	76.1	79.2	88.1	—	—	—	—
2.5 × 10 ⁻³	—	0.015 ± 0.001	0.047 ± 0.002	0.069 ± 0.003	0.12 ± 0.006	69.1	78.9	81.7	92.0	—	—	—	—
0	10	0.050 ± 0.001	0.045 ± 0.001	0.042 ± 0.002	0.04 ± 0.002	10.9	18.0	24.1	29.7	—	—	—	—
1 × 10 ⁻⁵	10	0.032 ± 0.001	0.117 ± 0.006	0.49 ± 0.029	0.64 ± 0.032	42.6	46.4	49.2	56.8	1.1	1.1	1.0	1.1
5 × 10 ⁻⁴	10	0.015 ± 0.001	0.048 ± 0.002	0.79 ± 0.015	0.22 ± 0.011	72.3	76.7	79.0	79.0	1.4	1.4	1.4	1.4
2.5 × 10 ⁻³	10	0.007 ± 0.0004	0.016 ± 0.001	0.026 ± 0.001	0.045 ± 0.002	86.8	90.1	93.09	96.9	2.1	1.8	2.2	2.1

Table 2. Weight loss measurement results for MS in 3.5% NaCl solution in the absence and presence of different concentrations of Glu(12)-2-Glu(12) and Glu(12)-2-Glu(12) + 10 mM KI at temperatures 30–60 °C.

Glu(12)-2-Glu(12) + KI, the presence of KI in Glu(12)-2-Glu(12) results in (i) a significant decrease in CMC, (ii) a decrease in γ_{CMC} (iii) higher value of π_{CMC} and (iv) the negatively higher value of ΔG_{ads}° . The combination of these results advocates that the adsorption of the Glu(12)-2-Glu(12) + KI gemini surfactant at the air/aqueous solution interface occurs more effectively than for the Glu(12)-2-Glu(12). This necessarily leads to the formation of a tightly packed monolayer film of the longer chain analogue at the air/aqueous solution interface, which is supported by the greater Γ_{cmc} value and thereby, the smaller A_{min} value. We also note here that the calculated ΔG_{ads}° value of the Glu(12)-2-Glu(12) surfactant is negatively larger than the corresponding ΔG_{mic}° value, indicating that the adsorption occurs predominantly over the micellization that is seen in aqueous solution. This supremacy of adsorption has similarly been reported in the earlier literatures focusing on the adsorption/micellization behavior of sugar-based gemini surfactants⁴¹.

Gravimetric Measurements

Effect of concentration and temperature. The corrosion parameters of mild steel in 3.5% NaCl solution in the absence and presence of different concentrations of Glu(12)-2-Glu(12) and Glu(12)-2-Glu(12) + 10 mM KI are summarized in Table 2. It can be examined that ν of mild steel in presence of Glu(12)-2-Glu(12) or Glu(12)-2-Glu(12) + 10 mM KI is both concentration and temperature dependent. With increase in Glu(12)-2-Glu(12) concentrations the corrosion rate decreases, which further decreases in presence of KI additive. This may be associated to the increased surface coverage of Glu(12)-2-Glu(12) at the mild steel/solution interface, which prevented the attack of 3.5% NaCl solution to mild steel surface and slowed down its dissolution. Glu(12)-2-Glu(12) in the presence of KI is observed to work more effectively. The improvement in the inhibition efficiency of Glu(12)-2-Glu(12) in the presence of KI can be explained on the basis of potential of zero charge and CMC lowering effect. The charge on the metal surface is determined from the value of $E_{corr} - E_{q=0}$, where $E_{q=0}$ is the zero charge potential. As reported in the literature, if $E_{corr} - E_{q=0} > 0$, the metal surface is positively charged⁴². In the present investigation, the obtained E_{corr} value of MS in 3.5% NaCl is -0.566 V (Ag/AgCl), whereas $E_{q=0}$ of iron in NaCl solution is reported to be -0.659 V (Ag/AgCl)⁴³. Thus the studied metal in NaCl solution is positively charged. The studied non-ionic surfactant is polar molecule having partial positive and partial negative sides. It has been proposed that halide ions are first adsorbed on the metal surface which leads to a recharging of the electrical double layer and the inhibitor is dragged into the double layer by electrostatic interaction with the adsorbed halide ions, forming ion-pairs directly on the surface of the metal. This ion-pair interaction consequently increases the surface coverage thereby reducing metal dissolution. The improvement in the inhibition efficiency of the studied inhibitor in presence of KI may be further explained on the basis of CMC lowering effect of gemini surfactant by the added salt⁴⁴. Generally, the surfactant having lower CMC values has greater adsorption capability^{45,46}. The addition of salt to the surfactants is known to decrease their solubility in the solution resulting in the formation of micelles at lower concentration and thus affecting the inhibition performance.

Effect of temperature is often used to determine whether an inhibitor is physically or chemically adsorbed on a metal surface to inhibit corrosion. An enhancement in inhibition efficiency with rise in electrolyte temperature is often associated with chemisorption phenomenon while the reverse signifies physisorption. To assess the effect of temperature on the corrosion inhibition of mild steel without and with Glu(12)-2-Glu(12) and Glu(12)-2-Glu(12) + KI, weight loss experiments were done at 30, 40, 50 and 60 °C using different concentration of Glu(12)-2-Glu(12). Inspection of Table 2 reveals that inhibition efficiencies increased with increase in solution temperature, confirming the ability of surfactants to inhibit corrosion of mild steel in NaCl solution at low and relatively high temperatures and supports chemisorption⁴⁷, which is more favoured at higher temperature because of lesser kinetic energy barrier. Further, at high temperatures, desorption of water molecules from the surface of steel is more, resulting in the larger surface area available for the adsorption of Glu(12)-2-Glu(12) gemini surfactant molecules. Also, an increase in the temperature of aqueous gemini surfactant solution increases the adsorption free energy thereby increasing the rate of adsorption on the MS surface⁴⁸.

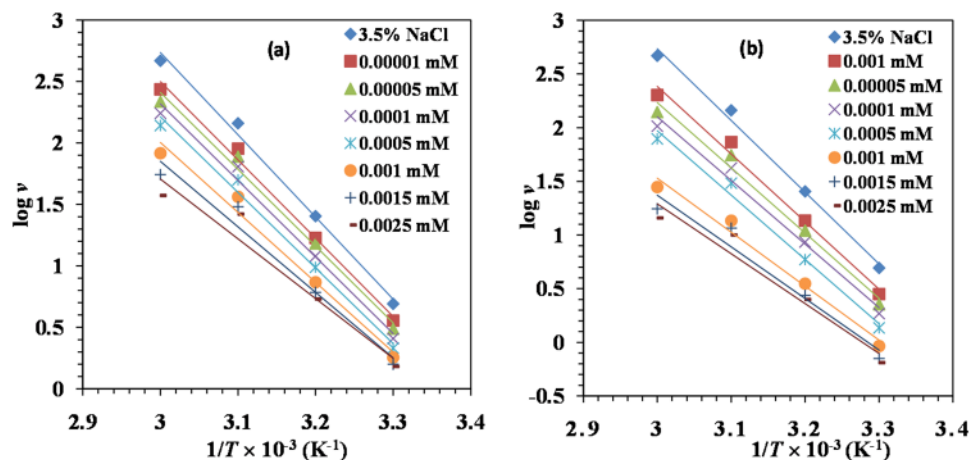


Figure 2. Arrhenius plots for MS in 3.5% NaCl in the absence and presence of different concentrations of (a) Glu(12)-2-Glu(12) and (b) Glu(12)-2-Glu(12) + 10 mM KI.

Synergistic effect of KI. To observe the effect of KI on the corrosion inhibition behaviour of Glu(12)-2-Glu(12), the corrosion of mild steel in 3.5% NaCl in absence and presence of varying concentration of Glu(12)-2-Glu(12) in combination with 10 mM of KI was separately studied in the temperature range of 30–60 °C by weight loss technique. It is clear that the mild steel corrosion is only slightly inhibited in the presence of either of a small concentration of Glu(12)-2-Glu(12) (1×10^{-5} mM) or KI (10 mM). But in the presence of Glu(12)-2-Glu(12) + 10 mM KI, ν shifted to lower values. For example, when 10 mM KI was added into the 3.5% NaCl solution containing 1×10^{-5} mM Glu(12)-2-Glu(12), ν decreased from $0.056 \text{ mg cm}^{-2} \text{ h}^{-1}$ to $0.032 \text{ mg cm}^{-2} \text{ h}^{-1}$. The greater $\eta_{w\%}$ shown in the presence of I^- ions may be due to its less degree of hydration as the adsorbability of anions is related to the degree of hydration and less hydrated ion is preferentially adsorbed on the metal surface. Accordingly, the $\eta_{w\%}$ increased from 69% to 86%, which could be attributed to adsorption of I^- ion over the corroded steel surface⁴⁹. The results suggest that there is a synergistic effect between inhibitor molecules and KI, which is judged by the synergism parameter, S_θ calculated using the following equations⁵⁰:

$$S_\theta = 1 - \theta_{1+2}/1 - \theta'_{1+2} \quad (12)$$

$$\theta_{1+2} = (\theta_1 + \theta_2) - (\theta_1\theta_2) \quad (13)$$

where θ_1 and θ_2 is the surface coverage by Glu(12)-2-Glu(12) and KI, respectively and θ'_{1+2} is the measured surface coverage by Glu(12)-2-Glu(12) + KI. In general, $S_\theta < 1$ implies an antagonistic behaviour, whereas $S_\theta > 1$ implies synergistic effect^{51,52}. The calculated values of S_θ are more than unity implying that the increased inhibition efficiency of Glu(12)-2-Glu(12) in presence of KI is only due to the synergistic effect (Table 2).

Kinetic considerations. In order to further elucidate the inhibitive properties of Glu(12)-2-Glu(12) gemini surfactant and the dependence of the temperature on the corrosion rate, the activation energy, E_a , enthalpy of activation, ΔH^* and entropy of activation, ΔS^* was calculated by Arrhenius equation and its alternative equation⁵² shown as equations (14) and (15). The relevant plots for mild steel corrosion in 3.5% NaCl in the absence and presence of various concentrations of Glu(12)-2-Glu(12) and Glu(12)-2-Glu(12) + KI at various temperatures are shown in Figs 2 and 3, respectively. The computed parameters are summarized in Table 3.

$$\log(\nu) = \log A - E_a/2.303RT \quad (14)$$

$$\nu = \frac{RT}{Nh} \exp\left(\frac{\Delta S^*}{R}\right) \exp\left(-\frac{\Delta H^*}{RT}\right) \quad (15)$$

where ν = corrosion rate, T = absolute temperature, R = universal gas constant. N = Avogadro number, and h = Planck's constant.

The lower values of E_a were observed for the inhibited systems than that for the uninhibited system indicating the chemical adsorption mechanism^{53,54}. The positive value of ΔH^* implies that the adsorption is endothermic reaction, which means it is good for adsorption when temperature is rising. The value of ΔH^* is lower than E_a , which means inhibitor has formed a stable layer on the steel surface⁵⁵. These results reflect that Glu(12)-2-Glu(12) is a good corrosion inhibitor. The negative value of ΔS^* for Glu(12)-2-Glu(12) can be explained in the following way: before the inhibitor molecules were adsorbed on the surface of mild steel, the molecules were scattered in the solution. However, as adsorption progressed the inhibitor molecules were orderly adsorbed on the surface, which led to a decrease in entropy⁵⁶.

Adsorption and thermodynamic considerations. The values of surface coverage, θ , computed from weight loss measurements were tested graphically by fitting to various adsorption isotherms models including

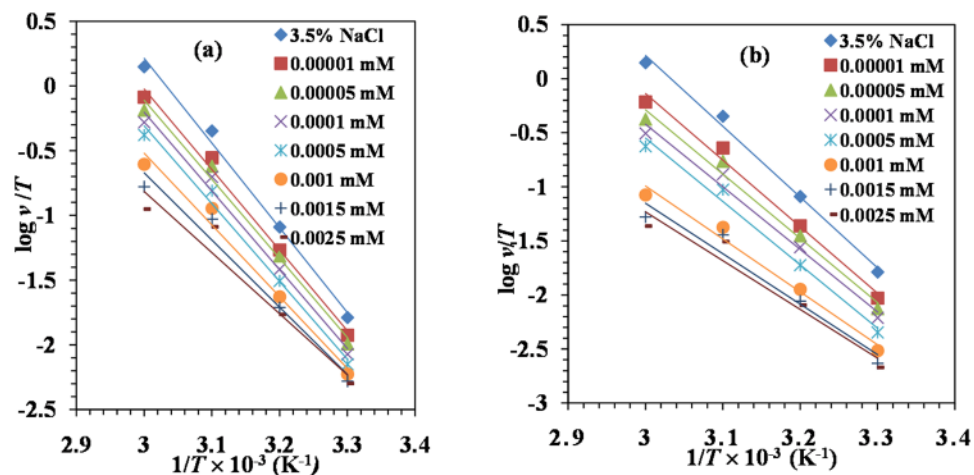


Figure 3. Alternative Arrhenius plots for MS in 3.5% NaCl in the absence and presence of different concentrations of Glu(12)-2-Glu(12) and Glu(12)-2-Glu(12) + 10 mM KI.

C (mM)	E_a (KJ mol ⁻¹)	ΔH^* (KJ mol ⁻¹)	ΔS^* (KJ mol ⁻¹ K ⁻¹)
3.5% NaCl	86.45	83.83	0.065
Glu(12)-2-Glu(12)			
1×10^{-5}	80.31	77.69	0.043
5×10^{-5}	78.12	75.50	0.034
1×10^{-4}	77.42	74.80	0.031
5×10^{-4}	76.17	64.59	0.024
1×10^{-3}	67.20	57.75	-0.006
1.5×10^{-3}	60.37	57.76	-0.029
2.5×10^{-3}	55.28	52.65	-0.047
Glu(12)-2-Glu(12) + KI			
1×10^{-5}	79.11	76.49	0.037
5×10^{-5}	76.15	73.53	0.025
1×10^{-4}	71.39	68.76	0.008
5×10^{-4}	70.41	67.78	0.002
1×10^{-3}	55.57	52.96	-0.050
1.5×10^{-3}	52.03	49.42	-0.063
2.5×10^{-3}	49.14	46.44	-0.074

Table 3. Activation parameters for corrosion of MS in 3.5% NaCl containing various concentrations of Glu(12)-2-Glu(12) and Glu(12)-2-Glu(12) + 10 mM KI inhibitor.

Langmuir, Temkin, Frumkin and Freundlich (Figs 4 and S2 (Supplementary Information)). The value of slopes and regression coefficient derived for different adsorption isotherms are given in Table S1 (Supplementary Information). The best adsorption isotherm in the present study was chosen based on the value of regression coefficient (R^2) for each tested isotherm. By far, the experimental data (R^2 were most close to one) for Glu(12)-2-Glu(12) or Glu(12)-2-Glu(12) + KI, best fitted the Langmuir isotherm (Fig. 4). The values of R^2 were used to determine the fitting of the experimental data to this unique isotherm. The isotherm is characterized by the mathematical model given below:

$$C/\theta = 1/K_{\text{ads}} + C \quad (16)$$

where, C = surfactant concentration, and K_{ads} = adsorption equilibrium constant that can be determined from the intercept of the straight line on the C/θ vs. C plot.

Linear plots were obtained for the different systems studied indicating that the experimental results relating the adsorption of Glu(12)-2-Glu(12) on mild steel can be approximated by Langmuir adsorption isotherm. The adsorption parameters derived from the plots are listed in Table 4. The K_{ads} (Table 4) values are high, suggesting the strong adsorption ability of Glu(12)-2-Glu(12) on the mild steel surface. The values of K_{ads} (Table 4) also indicate that the binding power of the inhibitor to the metal surface increases with rise in temperature.

The equilibrium constant of adsorption K_{ads} is related to the standard free energy of adsorption, $\Delta G_{\text{ads}}^\circ$ with the following equation:

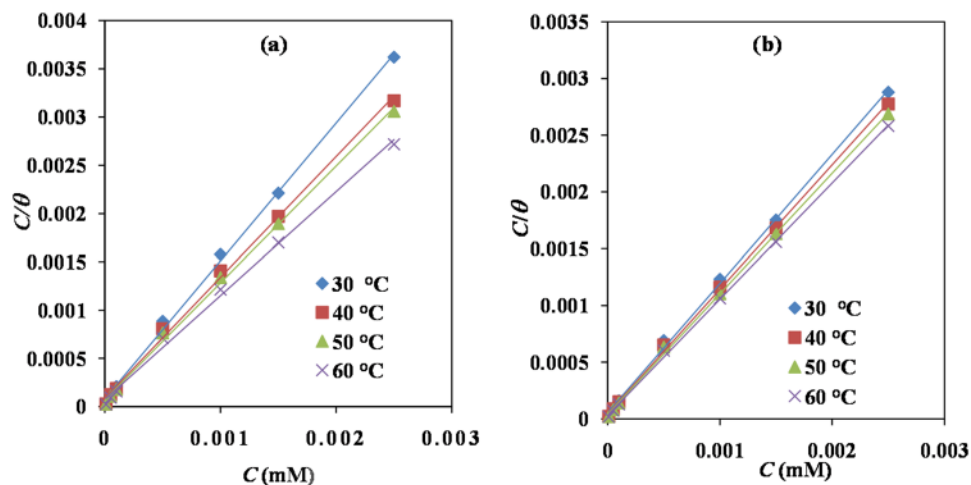


Figure 4. Langmuir adsorption isotherm plots for MS in 3.5% NaCl solution containing various concentrations of (a) Glu(12)-2-Glu(12) (b) Glu(12)-2-Glu(12) + 10 mM KI at 30–60 °C.

T (°C)	K_{ads} (mM ⁻¹)	ΔG_{ads}° (KJ mol ⁻¹)	ΔH_{ads}° (KJ mol ⁻¹)	ΔS_{ads}° (J mol ⁻¹ K ⁻¹)
Glu(12)-2-Glu(12)				
30	11111.11	-33.58	3.37	-0.121
40	11428.57	-34.77	3.37	-0.111
50	12048.19	-36.02	3.37	-0.111
60	12500.00	-37.23	3.37	-0.112
Glu(12)-2-Glu(12) + KI				
30	20000.00	-35.06	13.72	-0.161
40	22222.22	-36.49	13.72	-0.116
50	25000.00	-37.97	13.72	-0.117
60	33333.33	-39.95	13.72	-0.119

Table 4. Thermodynamic parameters of adsorption for MS in 3.5% NaCl at 30–60 °C.

$$K_{ads} = (1/55.5)\exp(-\Delta G_{ads}^{\circ}/RT) \quad (17)$$

where, R = universal gas constant and T = absolute temperature. The 55.5 value is the molar concentration of water in solution.

It has been demonstrated previously that higher the value of K_{ads} , the more easily is the inhibitor adsorbed on the metal surface³⁷, which means inhibitor has better inhibition performance. It can be seen from Table 4 that Glu(12)-2-Glu(12) + KI has the higher value of K_{ads} than Glu(12)-2-Glu(12) and thus Glu(12)-2-Glu(12) + KI outperforms Glu(12)-2-Glu(12) in inhibiting performance. The values of ΔG_{ads}° in the range of -20 – -40 KJ mol⁻¹ are assigned for the physical mode of adsorption. Meanwhile, ΔG_{ads}° values > -40 KJ mol⁻¹ are assigned for the chemical mode of adsorption⁵⁸. The values of ΔG_{ads}° , in the present investigation, range between -33.58 to -37.23 and -35.06 to -39.95 for Glu(12)-2-Glu(12) and Glu(12)-2-Glu(12) + KI, respectively, in the temperature range 30–60 °C, indicating that the process of adsorption of Glu(12)-2-Glu(12) onto the steel surface involve mixed physisorption and chemisorption with predominantly chemisorption mechanism.

Thermodynamic models are very useful tools in explaining the adsorption mechanism of inhibitor molecules onto a metal surface. Therefore, the heat of adsorption (ΔH_{ads}°) was assessed using the Van't Hoff equation:

$$\log K_{ads} = \frac{-\Delta H_{ads}^{\circ}}{2.303RT} + \text{constant} \quad (18)$$

where, ΔH_{ads}° and K_{ads} are the heat of adsorption and equilibrium constant of adsorption, respectively. Figure S3(a) (Supporting Information) shows the relationship between $\log K_{ads}$ and $1/T$ for Glu(12)-2-Glu(12) and the absorptive heat (ΔH_{ads}°) was approximated from the slope of the graph under the experimental conditions and presented in Table 4. The positive value of ΔH_{ads}° , displays the endothermic nature of the adsorption of the inhibitor molecules on the mild steel surface. Generally the endothermic process is attributable unequivocally to chemisorption⁵⁹.

Another thermodynamic parameter, entropy of adsorption (ΔS_{ads}°) was calculated using basic thermodynamic equation:

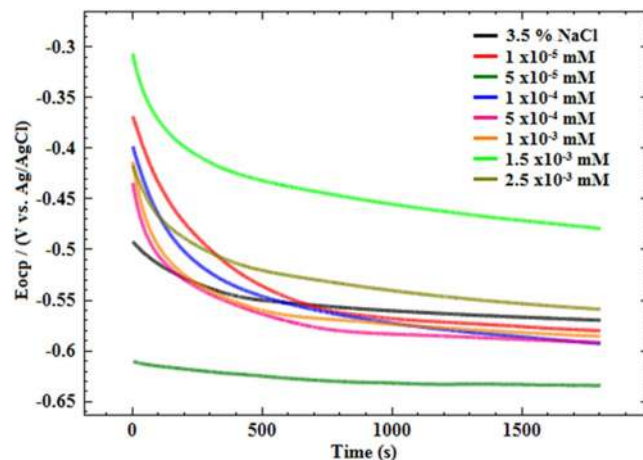


Figure 5. Variation of E_{OCP} -time curves for MS in uninhibited and inhibited 3.5% NaCl solution (temperature $30 \pm 2^\circ\text{C}$).

$$\Delta G_{\text{ads}}^{\circ} = \Delta H_{\text{ads}}^{\circ} - T\Delta S_{\text{ads}}^{\circ} \quad (19)$$

Values of $\Delta S_{\text{ads}}^{\circ}$ ranges between -0.12 – 0.11 KJ mol^{-1} (Table 4) were obtained by substitution of corresponding values of other thermodynamic values at 30 – 60°C . The negative value of $\Delta S_{\text{ads}}^{\circ}$ for Glu(12)-2-Glu(12) can be explained by the following way: before adsorbing on the metal surface, the inhibitor molecules were in scattered manner in the solution, but in the process of adsorption, inhibitor molecules were orderly adsorbed on the mild steel surface, which led to decrease in entropy^{28,59}.

Electrochemical Study

Open circuit potential. As shown in Fig. 5, the OCP curves have similar shapes and the approximate variation trend. E_{OCP} changes to a positive direction at initial 320 s immersions, and then reaches a steady state after 500 s immersion. Without inhibitor, the mild steel had an E_{OCP} about -0.57 V vs. Ag/AgCl. For 1×10^{-5} mM Glu(12)-2-Glu(12), the value of E_{OCP} was changed to -0.59 V vs. Ag/AgCl. The negative shift in E_{OCP} values indicated that the Glu(12)-2-Glu(12) molecules retarded mainly the cathodic corrosion process of mild steel corrosion in 3.5% NaCl solution. The similar curves were obtained for Glu(12)-2-Glu(12) + KI (not shown here).

Potentiodynamic polarization measurement. Figure 6(a,b) shows potentiodynamic polarization curves for mild steel in 3.5% NaCl, both in the presence and absence of Glu(12)-2-Glu(12) and Glu(12)-2-Glu(12) + 10 mM KI at a range of concentrations. Various polarization parameters including corrosion potential (E_{corr}), anodic (β_a) and cathodic (β_c) Tafel slopes, corrosion current density (i_{corr}), and the calculated inhibition efficiency (η_i) values are given in Table 5.

The variation in the values of β_c and β_a in the presence of Glu(12)-2-Glu(12) and Glu(12)-2-Glu(12) + 10 mM KI indicate that both the anodic metal dissolution and cathodic hydrogen evaluation processes are inhibited. From Table 5, it is also observed that β_a and β_c values of the inhibited acid solutions are smaller compared to that of the uninhibited solution, but does not follow a specific pattern with increase in inhibitor concentration. This suggests that the corrosion reaction mechanism is not modified⁶⁰ due to the presence of Glu(12)-2-Glu(12). It is reported in the literature that, if the displacement in E_{corr} is more than 85 mV with respect to E_{corr} of the blank, the inhibitor can be classified as cathodic or anodic type otherwise it is of mixed type inhibitor⁶¹. From Table 5, it can be seen that the addition of Glu(12)-2-Glu(12) causes shift in the values of E_{corr} of the inhibited systems in relation to the uninhibited solution is <85 mV qualifying it as mixed type inhibitor. The value of i_{corr} decreases with increasing Glu(12)-2-Glu(12) concentrations, which is further decreased in presence of KI additive. For instance, the presence of 2.5×10^{-3} mM of Glu(12)-2-Glu(12) caused a decrease in i_{corr} from $0.21 \pm 0.02 \times 10^{-4}$ A.cm^{-2} (for 3.5% NaCl solution) to $0.04 \pm 0.003 \times 10^{-4}$ A.cm^{-2} , which further decreased to $0.036 \pm 0.003 \times 10^{-4}$ A.cm^{-2} in presence of 10 mM KI. The decrease in i_{corr} values is due to the adsorption of the inhibitor molecules, which blocked the active sites on the mild steel surface. Thus, the free surface area for H^+ ions reduction was decreased while the actual reaction mechanism remains unaffected⁶².

Electrochemical impedance spectroscopy. Figures 7 and 8, shows Nyquist and Bode modulus plots for mild steel corrosion in 3.5% NaCl solution without and with various concentrations of Glu(12)-2-Glu(12) and Glu(12)-2-Glu(12) + 10 mM KI at 30°C . The impedance parameters are shown in Table 6. In the presence of Glu(12)-2-Glu(12) and Glu(12)-2-Glu(12) + 10 mM KI, the profile of impedance diagrams, which are almost semi-circle does not alter. This implies that in the investigated environment the corrosion of mild steel is mainly controlled by a charge transfer process⁶³. The deviation from perfect circular shape is associated with heterogeneity of the working electrode and presence of micro roughness⁶⁴. The inhibitor, Glu(12)-2-Glu(12) or Glu(12)-2-Glu(12) + 10 mM KI inhibited the mild steel corrosion in 3.5% NaCl solution is evident from the fact that

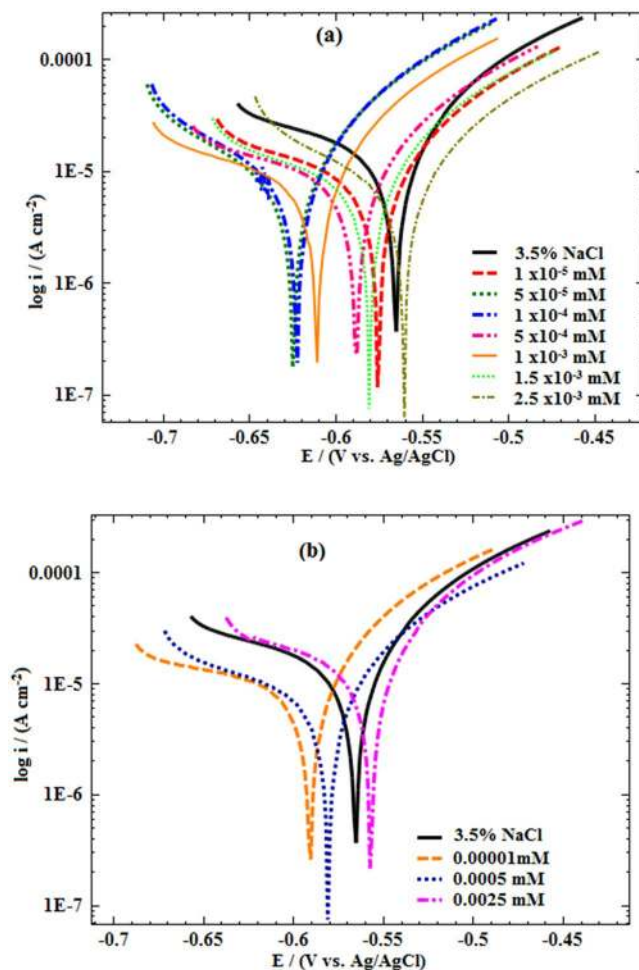


Figure 6. Potentiodynamic polarization curves of MS in 3.5% NaCl solution without and with different concentrations of (a) Glu(12)-2-Glu(12) (b) Glu(12)-2-Glu(12) + 10 mM KI.

C (mM)	E_{corr} (V vs. Ag/AgCl)	β_a (V dec ⁻¹)	β_c (V dec ⁻¹)	$i_{corr} \times 10^{-4}$ (A cm ⁻²)	η_i (%)
3.5% NaCl	-0.566	0.305	0.073	0.21 ± 0.02	—
Glu(12)-2-Glu(12)					
1×10^{-5}	-0.576	0.252	0.107	0.16 ± 0.005	23.6
5×10^{-5}	-0.624	0.298	0.068	0.12 ± 0.007	40.0
1×10^{-4}	-0.623	0.193	0.062	0.11 ± 0.004	45.3
5×10^{-4}	-0.589	0.151	0.056	0.09 ± 0.004	60.2
1×10^{-3}	-0.611	0.080	0.070	0.08 ± 0.005	62.7
1.5×10^{-3}	-0.580	0.117	0.053	0.072 ± 0.001	65.6
2.5×10^{-3}	-0.508	0.330	0.248	0.04 ± 0.003	79.5
Glu(12)-2-Glu(12) + KI					
1×10^{-5}	-0.604	0.279	0.054	0.098 ± 0.002	53.2
5×10^{-4}	-0.581	0.117	0.053	0.07 ± 0.002	66.6
2.5×10^{-3}	-0.557	0.021	0.019	0.043 ± 0.003	83.1

Table 5. PDP Parameters for MS in 3.5% NaCl in the absence and presence of different concentrations of Glu(12)-2-Glu(12) and Glu(12)-2-Glu(12) + 10 mM KI at 30 °C.

compared with uninhibited system the semicircles of Nyquist diagrams of inhibited systems are larger in size. The above effect, which is a function of inhibitor concentration, is also evident from Bode modulus and phase angle plots where in comparison to 3.5% NaCl solution the impedance and phase angles have shifted toward greater values in inhibitor containing solutions.

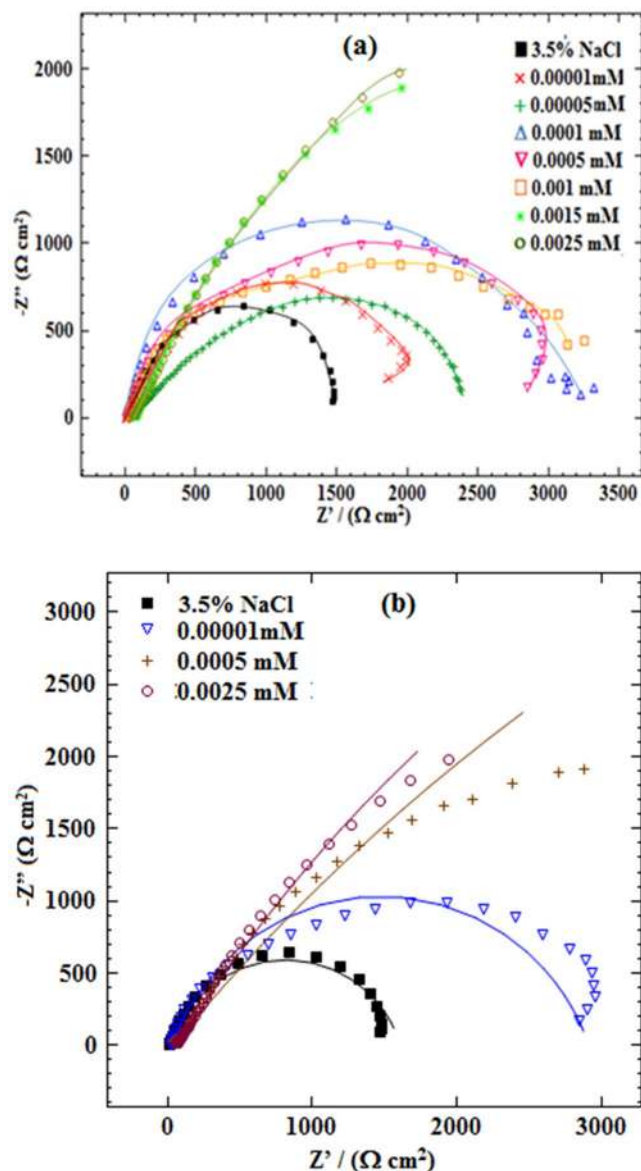


Figure 7. Nyquist plots of MS in 3.5% NaCl solution without and with different concentrations of (a) Glu(12)-2-Glu(12) (b) Glu(12)-2-Glu(12) + 10 mM KI.

For the analysis of the impedance spectra of Glu(12)-2-Glu(12), an appropriate equivalent circuit shown in Fig. S4 (Supporting Information) was used, which consists of the parallel combination of a capacitor, C_{dl} and a charge transfer resistor, R_{ct} in series with a solution resistor R_s . A good fit with this model was obtained with our experimental data (Figs 7 and 8a,b). It is observed that the fitted data match with the experimental data, with the low chi-square (χ^2) value (see Table 6). In the fitted Nyquist and Bode plots, Figs 7 and 8(a,b), the symbols depicts the experimental data, while solid lines show the best fits. The pure electric models can verify mechanistic models and approves the calculation of numerical values corresponding to the physical and/or chemical properties of the electrochemical system under investigation. The proposed circuit allows the identification of both the solution resistance and charge transfer resistance. The capacitance value is affected by defects of the surface, which can be simulated via a constant phase element (CPE)⁶⁵. The CPE is determined by a component Y_0 and a coefficient n , where n quantifies different physical phenomena, like surface in-homogeneity arising from surface roughness, inhibitor adsorption, porous layer formation, etc. In this case, the capacitance is calculated by the following mathematical formulation:

$$C_{dl} = Y_0(2\pi f_{max})^{n-1} \quad (20)$$

where, f_{max} represents the frequency at which the imaginary component of the impedance is maximal on the Nyquist plot.

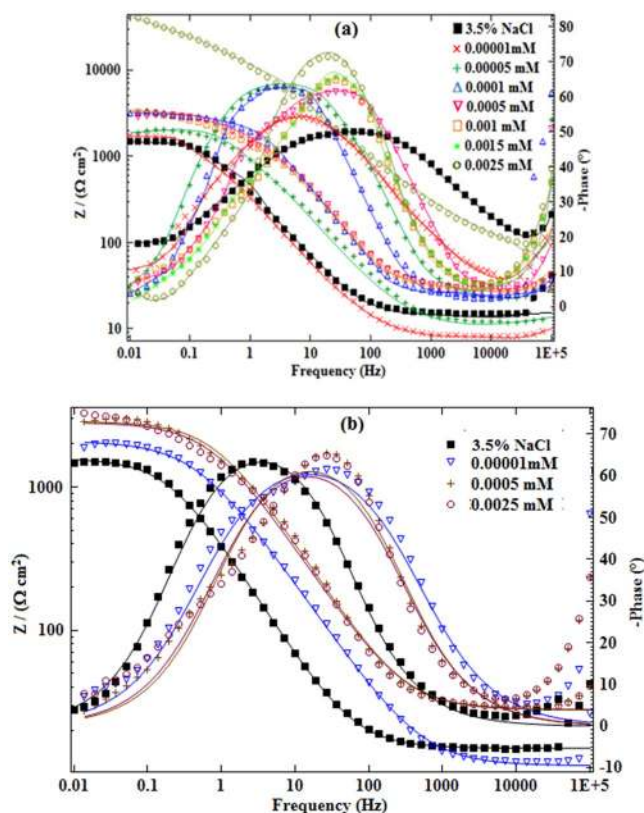


Figure 8. Bode plots of MS in 3.5% NaCl solution without and with different concentrations of inhibitors (a) Glu(12)-2-Glu(12) (b) Glu(12)-2-Glu(12) + 10 mM KI.

C (mM)	R_s (Ω cm ²)	R_{ct} (Ω cm ²)	$\chi^2 \times 10^{-3}$	CPE		$C_{dl} \times 10^{-4}$ (F cm ⁻²)	η_R (%)
				$Y_0 \times 10^{-4}$ ($\Omega^{-1} s^n$ cm ⁻²)	n		
3.5% NaCl	18.77	1541 ± 60.1	2.3	4.85	0.9877	4.83	—
Glu(12)-2-Glu(12)							
1×10^{-5}	11.37	2138 ± 87.6	2.5	1.64	0.9914	1.62	27.9
5×10^{-5}	85.13	2573 ± 23.1	1.5	1.04	0.9929	1.03	40.1
1×10^{-4}	65.98	3176 ± 60.3	2.7	0.47	0.9964	0.47	51.4
5×10^{-4}	68.44	3516 ± 101.3	5.7	0.43	0.9979	0.43	56.1
1×10^{-3}	52.97	4037 ± 48.0	2.1	0.39	0.9981	0.39	61.8
1.5×10^{-3}	37.61	4537 ± 186.0	1.9	0.30	0.9984	0.30	66.0
2.5×10^{-3}	32.64	5709 ± 62.8	2.1	0.28	0.9988	0.27	73.0
Glu(12)-2-Glu(12) + KI							
1×10^{-5}	10.36	2621 ± 33.9	2.2	1.11	0.9973	1.1	41.2
5×10^{-4}	81.01	5636 ± 84.5	3.1	0.28	0.9982	0.28	72.6
2.5×10^{-3}	77.77	8857 ± 203.7	1.6	0.18	0.9998	0.18	82.6

Table 6. EIS parameters and inhibition efficiency of MS in 3.5% NaCl in absence and presence of varying concentrations of Glu(12)-2-Glu(12) and Glu(12)-2-Glu(12) + 10 mM KI at 30 °C.

At 2.5×10^{-3} mM of studied inhibitor, the addition of KI gives a R_{ct} value of $8857 \pm 203.7 \Omega$ cm² and C_{dl} value of $0.18 \times 10^{-4} \mu$ Fcm⁻², while Glu(12)-2-Glu(12) gives respective values of $5709 \pm 62.8 \Omega$ cm² and $0.27 \times 10^{-4} \mu$ Fcm⁻². Under any given conditions, R_{ct} Glu(12)-2-Glu(12) + KI > R_{ct} Glu(12)-2-Glu(12), while C_{dl} Glu(12)-2-Glu(12) + KI < C_{dl} Glu(12)-2-Glu(12), implying improved inhibition by Glu(12)-2-Glu(12) + KI than by Glu(12)-2-Glu(12). In both cases, generally, η_R increases with the concentration of the inhibitor, and follows the order: η_R Glu(12)-2-Glu(12) + KI > η_R Glu(12)-2-Glu(12).

In Fig. 8(a,b), the Bode-phase angle diagrams for mild steel with and without various concentrations of Glu(12)-2-Glu(12) and Glu(12)-2-Glu(12) + KI are shown. The increase in the absolute value of impedance $|Z|$ at low frequencies confirms the corrosion protection offered by the studied inhibitor because when the inhibitor is added, there is an increase in the impedance value of one order of magnitude. The increase of the phase angle in

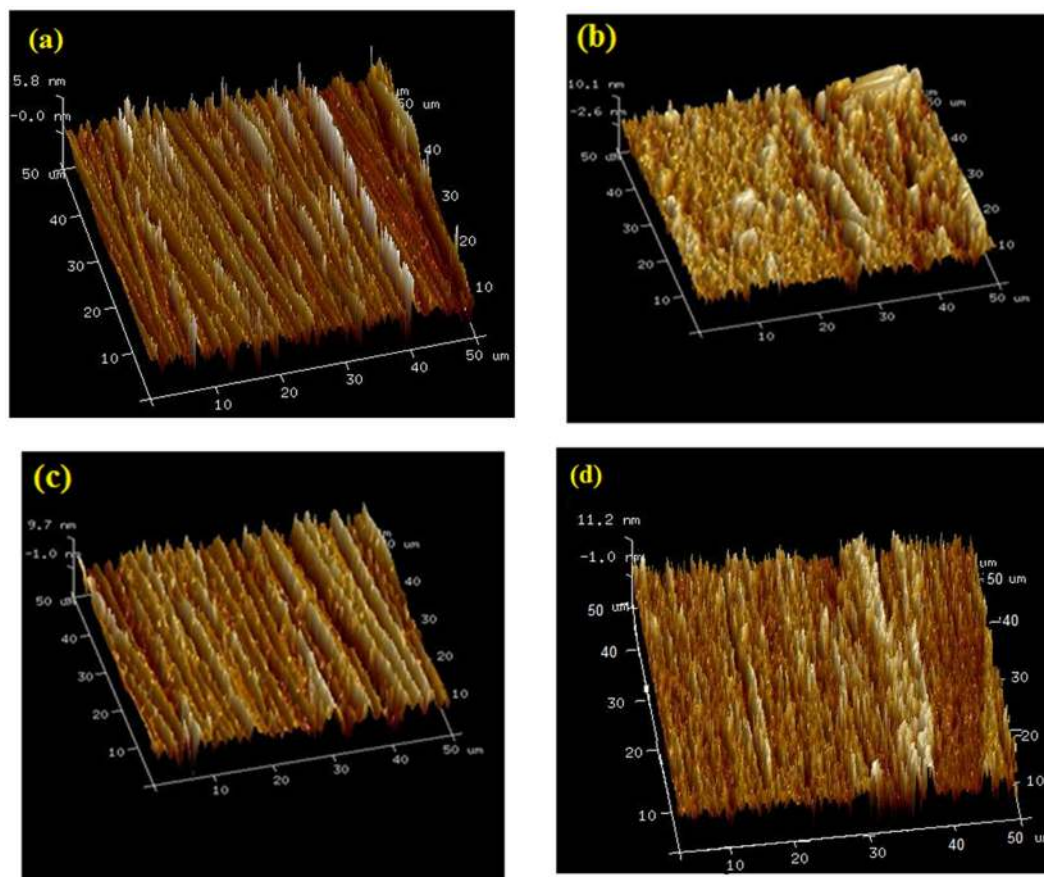


Figure 9. AFM images of MS after 6 h immersion: **(a)** polished MS prior to immersion, **(b)** MS in 3.5% NaCl solution, **(c)** MS in 3.5% NaCl solution with 2.5×10^{-3} mM Glu(12)-2-Glu(12), **(d)** in 3.5% NaCl solution with 2.5×10^{-3} mM Glu(12)-2-Glu(12) + 10 mM KI.

the presence of the inhibitor indicates that it is adhering to the metallic surface⁶⁶. Additionally, one time constants could clearly be observed for all concentrations.

Surface characterization. AFM was used to get the 3-D topography of mild steel specimen. Analysis of the AFM results allowed the quantification of surface roughness over an area of $50 \mu\text{m} \times 50 \mu\text{m}$. The 3-D AFM images are shown in Fig. 9(a–d). Figure 9(a) shows the mild steel surface before to immersion, which looks smooth and uniform. The mild steel surface in the uninhibited NaCl solution has become quite rough (Fig. 9b) due to the unhindered attack of the corrosive solution. However, in the presence of optimum concentration of the Glu(12)-2-Glu(12) and Glu(12)-2-Glu(12) + 10 mM KI (Fig. 9c,d), the roughness is greatly diminished in comparison to that in the absence of inhibitor. The average surface roughness of the mild steel before immersion is 81 nm, which is raised to 447 nm after immersion in uninhibited 3.5% NaCl solution. In the presence of Glu(12)-2-Glu(12) and Glu(12)-2-Glu(12) + KI, the roughness decreased to 154 nm and 129 nm, respectively. The results are further supported by height profiles graphs (Fig. 10). In comparison to the coupon immersed in 3.5% NaCl solution, which is shown to exhibit uneven height profile, the coupons immersed in inhibited NaCl solution have smoother height profile curve.

The surface morphologies of freshly polished mild steel surface and mild steel surface immersed in the corrosive solutions for 6 h in the absence and presence of optimum concentration of the studied inhibitor are shown in Fig. 11(a–d). The freshly polished mild steel shows smooth, non-corroded surface with polishing scratches (see Fig. 11a). The mild steel retrieved from 3.5% NaCl without the inhibitor exhibits strongly damaged and corroded surface due to direct attack in the uninhibited corrosive environment (Fig. 11b). It is manifested from Fig. 11(c,d) that the mild steel specimens immersed in the inhibited aggressive solution are only slightly damaged compared to the one recovered from 3.5% NaCl solution. This is a sign of the existence of an inhibitive film of the Glu(12)-2-Glu(12) molecules on the steel surface thereby shielding it from direct attack. In the presence of combined Glu(12)-2-Glu(12) + KI (Fig. 10d), the steel specimen has a better morphology and smooth surface compared with that of the surface immersed in Glu(12)-2-Glu(12) solution. A comparatively lesser destruction of the mild steel surface might be due to the specific adsorption of I^- ions on the mild steel which facilitates the adsorption of Glu(12)-2-Glu(12) molecules.

In order to confirm the composition of corrosion products formed on the mild steel surface, the surface of specimens before and after 6 h immersion in the uninhibited and inhibited (inhibitor concentration 2.5×10^{-3}

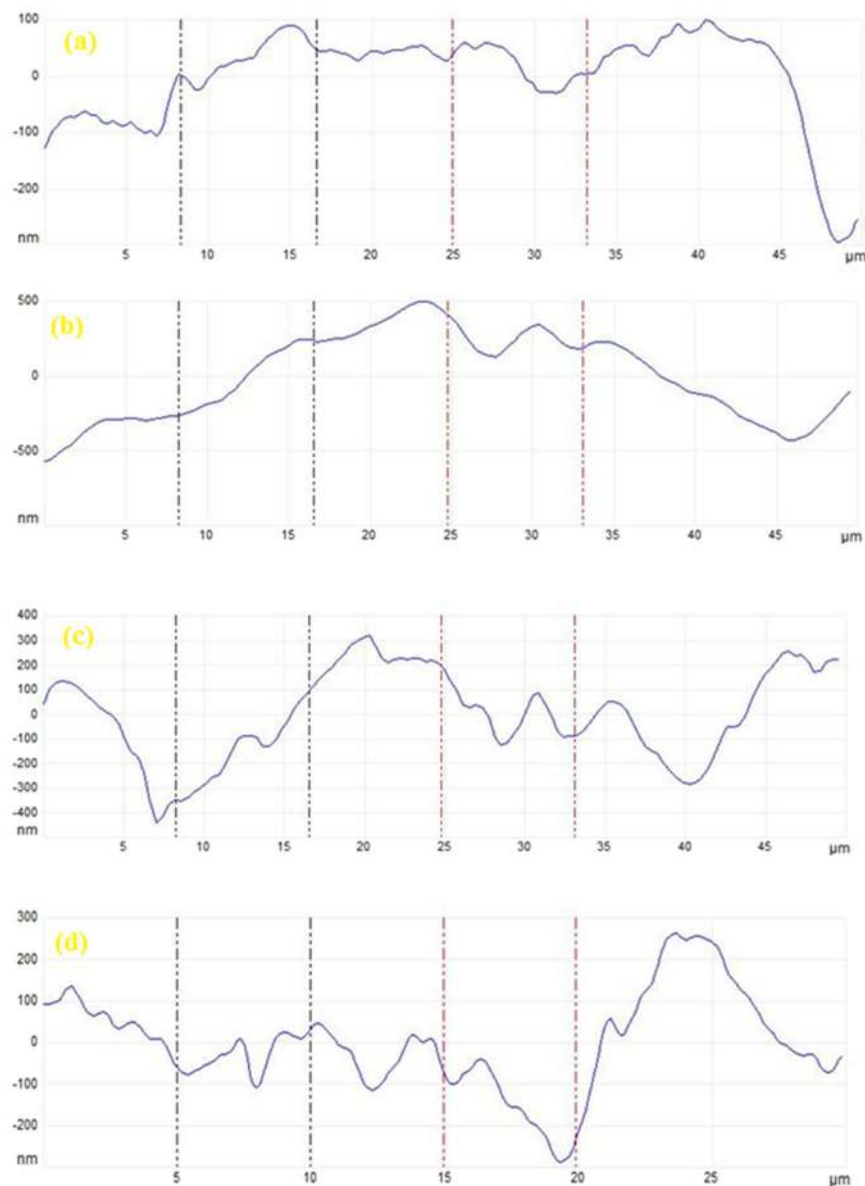


Figure 10. Height profile images of the MS surface (a) polished MS prior to immersion (b) MS in 3.5% NaCl solution (c) MS in 3.5% NaCl solution with 2.5×10^{-3} mM Glu(12)-2-Glu(12) (d) MS in 3.5% NaCl solution with 2.5×10^{-3} mM Glu(12)-2-Glu(12)+10 mM KI.

mM) 3.5% NaCl solution was analyzed using EDAX. The results of the EDAX analysis are shown in Fig. S5(a–d) (Supporting Information). The surface of mild steel prior to suspension in the 3.5% NaCl solution shows an intense peak of Fe along with the peaks of other elements constituting the mild steel (Fig. S5(a) supporting information). The EDAX spectrum obtained after the immersion of the mild steel in the 3.5% NaCl solution exhibits the additional peaks of Cl (Fig. S5(b) supporting information), which is ascribed to the free corrosion of unprotected mild steel in the 3.5% NaCl solution. Due to unhindered corrosion of mild steel the peak of Fe is highly suppressed. An additional and prominent peak of O, which was absent in Fig. S5(a) (Supporting Information), was evident due to the formation of complex oxides/hydroxides on the surface. The corrosion of mild steel has also resulted in the loss of some of the elements making the steel. In the presence of the inhibitor Glu(12)-2-Glu(12), the peak of Cl is absent and an additional peak of N (due to N atoms from the inhibitor) is present (Fig. S5(c) Supporting Information). This is associated to the absence of corrosion due to the formation of a protective adsorption film having N covering on the mild steel surface. As a result of the formation of a protective covering the intensity of the Fe peak is also enhanced whereas the intensity of O peak is lowered. In presence of Glu(12)-2-Glu(12) + KI (Fig. S5(d) Supporting Information), the extent of corrosion is further lowered and some of the peaks (e.g. Mn and Si) lost due to corrosion reappears.

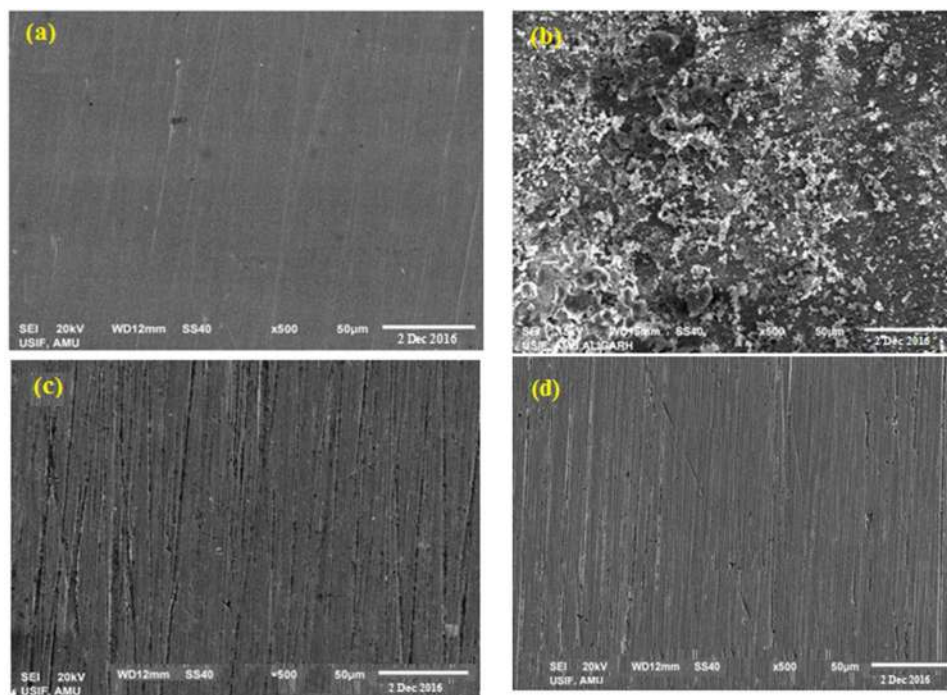


Figure 11. SEM images of the MS after 6 h immersion in 3.5% NaCl solution: (a) polished MS prior to immersion, (b) MS in 3.5% NaCl solution, (c) MS in 3.5% NaCl solution with 2.5×10^{-3} mM Glu(12)-2-Glu(12) (d) MS in 3.5% NaCl solution with 2.5×10^{-3} mM Glu(12)-2-Glu(12) + 10 mM KI.

Quantum chemical calculations. Quantum chemical calculations were performed to explore the relationship between electronic structure of the Glu(12)-2-Glu(12) and its inhibition ability. Optimized structures, the highest occupied molecular orbital (HOMO) and the lowest unoccupied molecular orbital (LUMO) density distribution of studied inhibitors are presented in Fig. 12(a–c). Indeed, some calculated quantum chemical indices including E_{HOMO} , E_{LUMO} , ΔE , I , A , χ , η , and ΔN are given in Table 7. The trends of properties obtained using different basis sets are the same (Table 7).

According to the frontier molecular orbital theory, the formation of a transition state occurs due to interactions between the frontiers orbitals (HOMO and LUMO) of the reactants⁶⁷. The HOMO is linked with the ability of an inhibitor molecule to give electrons and to bond to a metal surface. Higher values of E_{HOMO} indicate that a molecule is more likely to give electrons to appropriate acceptor molecules. In contrast, the LUMO exhibits the electron accepting ability of a molecule, with lower values of E_{LUMO} implying a higher electron accepting ability⁶⁸. Glu(12)-2-Glu(12) adsorbed on the mild steel surface due to the interaction of partially filled d orbital $\{[\text{Ar}] 4s^2 3d^6\}$ of iron atoms and unshared electron pairs in nitrogen and oxygen. The HOMO of Glu(12)-2-Glu(12) could bond with the partially filled 3d orbital of iron atom while the LUMO of Glu(12)-2-Glu(12) could interact with the 4s orbital of iron atom. As the ΔE reflects the stability of a molecule, smaller values of ΔE indicate that a molecule could potentially be adsorbed more easily on a metal surface. As ΔE decreases, the reactivity of a molecule towards a metal surface increases, thus leading to enhancement of the inhibition efficiency of the molecule^{38,69}.

The values of E_{HOMO} and E_{LUMO} of the inhibitor molecule are association with I and A , respectively⁷⁰. The values of I and A are defined as $-E_{\text{HOMO}}$ and $-E_{\text{LUMO}}$, respectively and the obtained values are used to calculate η and χ .

$$\eta = \frac{I - A}{2} \quad (21)$$

$$\chi = \frac{I + A}{2} \quad (22)$$

Calculated values of χ are also mentioned in Table 7, which denotes the tendency of an atom to attract the shared pair of electron towards itself. The values of η determines both the stability and reactivity of a molecule which suggests the resistivity of the inhibitor for the physical adsorption process. Soft molecules with small energy gaps are far more reactive than hard ones with large energy gaps, as they could readily offer electrons to an acceptor.

The fraction of electrons transferred⁷¹ (ΔN) from the inhibitor to MS surface can be calculated by using χ and η values, is calculated according to equation (23).

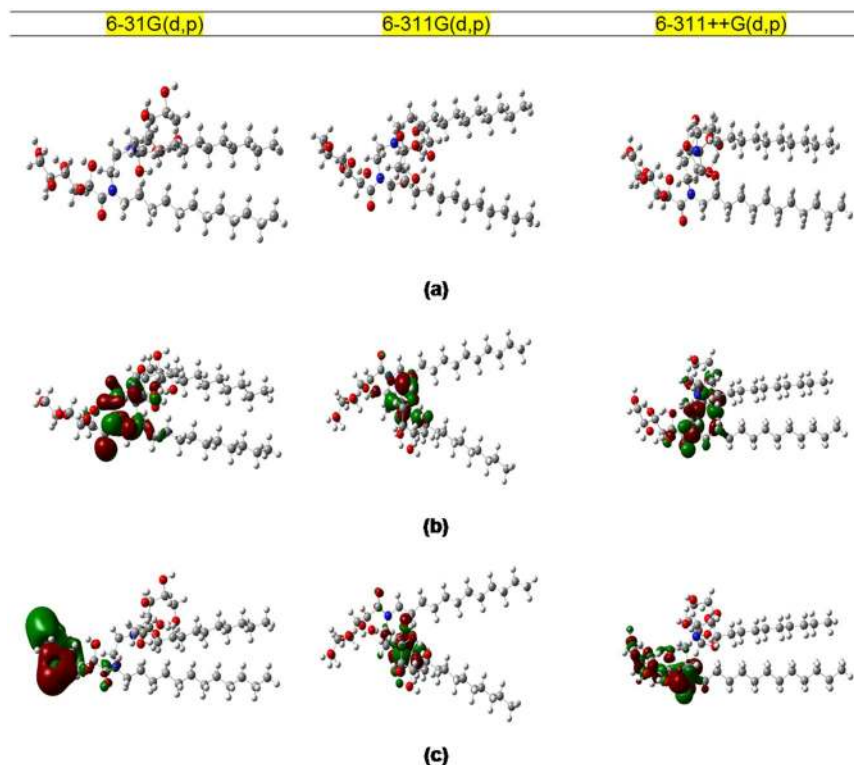


Figure 12. Quantum chemical results of Glu(12)-2-Glu(12) molecule obtained by DFT method at B3LYP with 6-31G (d, p), 6-311G (d, p) and 6-311G++ (d, p) basis set: (a) optimized molecular structure, (b) HOMO, (c) LUMO.

	6-31G(d, p)	6-311G(d, p)	6-311++G(d, p)
E_{HOMO}	-3.256	-2.807	-2.227
E_{LUMO}	3.995	3.110	1.128
ΔE	7.252	5.917	3.356
I	3.256	2.807	2.228
A	-3.995	-3.110	-1.128
χ	-3.626	-0.152	0.549
η	3.626	2.958	1.677
ΔN	0.715	0.840	1.272

Table 7. Calculated quantum chemical parameters of the studied inhibitor using the DFT method at B3LYP with 6-31 G (d, p), 6-311 G (d, p) and 6-311 G++ (d, p) basis sets.

$$\Delta N = \frac{\chi_{\text{Fe}} + \chi_{\text{inh}}}{2(\eta_{\text{Fe}} + \eta_{\text{inh}})} \quad (23)$$

where χ_{Fe} and χ_{inh} represent the electronegativity and the η_{Fe} and η_{inh} represent the absolute hardness of iron and the inhibitor molecules, respectively. The theoretically calculated value of χ_{Fe} for iron metal is 7 eV mol^{-1} and the η_{Fe} is 0 eV mol^{-1} . These values are appropriately substituted to calculate ΔN . Recently, several researchers⁷¹⁻⁷³ reported that the incorporation of 7 eV mol^{-1} as the magnitude of χ_{Fe} is conceptually incorrect as it is only related to free electron gas Fermi energy of Fe atom in which the interactions among the electrons had not been considered. Thus work function (ϕ) of the metal surface instead of χ_{Fe} , is used, as it is more appropriate measure for its electronegativity. Therefore, equation 23 is rewritten as follows.

$$\Delta N = \frac{\phi - \chi_{\text{inh}}}{2(\eta_{\text{Fe}} + \eta_{\text{inh}})} \quad (24)$$

The obtained DFT derived ϕ value for Fe(110) plane is 4.82 eV ⁷². These values are appropriately substituted to calculate ΔN . Values of ΔN exhibit the path of the electron transfer between inhibitor and metal surface. The ΔN

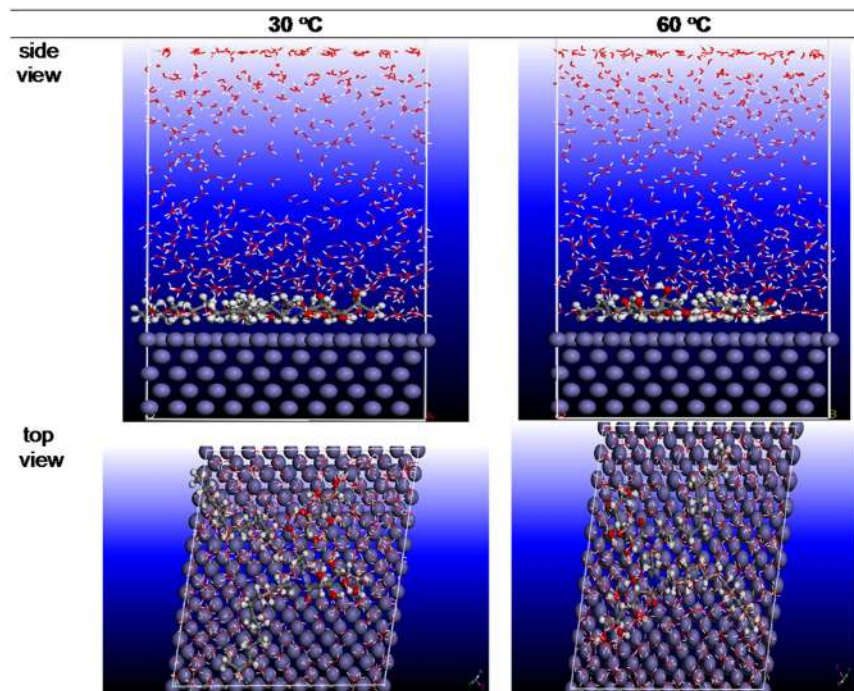


Figure 13. Equilibrium adsorption configurations of Glu(12)-2-Glu(12) on the Fe (110) surface at 30 and 60 °C obtained by MD simulation.

System	30 °C		60 °C	
	$E_{\text{interaction}}$ (kJ/mol)	E_{binding} (kJ/mol)	$E_{\text{interaction}}$ (kJ/mol)	E_{binding} (kJ/mol)
Fe (110)/Inh/500H ₂ O	-503.77	503.77	-684.41	684.41

Table 8. Selected energy parameters obtained from MD simulations for adsorption of inhibitor on Fe(110) surface.

exhibit the inhibitive performance of the inhibitors resulted from electron donations. In the current investigation, ΔN values are greater than zero indicating electron transfer from the inhibitor to the MS surface²⁸.

MD Simulations

Because strong correlation exists between electronic properties of inhibitor and corrosion effectiveness, DFT calculations are very useful for the overall understanding of electronic properties of corrosion inhibitors. On the other side, understanding the interactions of inhibitor molecules with metal surface is also of great importance. In this case, MD simulations can be particularly useful for the understanding of corrosion inhibition process. In the current study, the binding and interaction energies of the adsorbed inhibitor have been approximated when the simulation system reached their equilibrium state⁷². The best adorable top and side views of adsorption configuration of the studied molecule on Fe(110) surface at 30 to 60 °C is shown in Fig. 13 while the interaction and binding energies at both temperatures are placed in Table 8. Looking at Fig. 13, what stands out is that inhibitor molecule at both temperatures had been moved in nearly parallel or flat disposition which provide larger blocking area by inhibitor molecule preventing the surface from corrosion through a formation of a barrier layer between the metal surface and the aggressive media. The large negative values of the interaction energies for both temperatures indicating that the interaction between inhibitor molecules and Fe(110) surface is spontaneous, strong and stable⁷⁴. On the other hand, the high magnitude of the binding energies suggesting that the adsorption system is more stable and that there is more than one bond to the iron surface per inhibitor molecule⁷⁵. The presence of many reactive sites, i.e. hydroxyl groups, nitrogen atoms as well as carbon chains in the inhibitor molecule caused highly improved inhibitive properties. Furthermore, the increase of the temperature from 30 to 60 °C increases the interactive forces of the inhibitor, in accordance with experimental results.

Conclusions

1. The corrosion of mild steel in 3.5% NaCl has been inhibited by the addition of Glu(12)-2-Glu(12) and KI.
2. Significant improvement in inhibiting efficiency was observed in the presence of the mixture of Glu(12)-2-Glu(12) and KI. The inhibition efficiency was enhanced to 97% and showed a synergism of inhibition.

- Glu(12)-2-Glu(12)+KI synergistic inhibitor system was found to be an excellent and cost-efficient inhibitor for mild steel corrosion in NaCl solution.
- The values of S_0 are greater than unity showing the corrosion inhibition brought about by Glu(12)-2-Glu(12) in combination with the KI is synergistic in nature and co-operative adsorption between halides and Glu(12)-2-Glu(12) prevails over competitive adsorption.
- According to E_{corr} of both the systems, Glu(12)-2-Glu(12) and Glu(12)-2-Glu(12) + KI affected both anodic and cathodic reactions so can be classified as mixed type inhibitor.
- SEM images show that the best morphology surface is obtained for Glu(12)-2-Glu(12) + KI inhibitor.
- AFM images showed that the molecules of Glu(12)-2-Glu(12) + KI protect the mild steel surface and prevent it from having direct contact with corrosive ions.
- Experimental findings were adequately supported by quantum chemical calculations.
- The configuration of molecules on metal surface was simulated using MD. The results reveal that Glu(12)-2-Glu(12) adsorbed onto the mild steel surface in a nearly parallel or flat disposition with large negative values of the interaction energies for both temperatures indicating that the interaction between inhibitor molecules and Fe(110) surface is spontaneous, strong and stable.

References

- Guo, W., Chen, S., Feng, Y. & Yang, C. Investigations of triphenyl phosphate and bis-(2-ethylhexyl) phosphate self-assembled films on iron surface using electrochemical methods, Fourier transform infrared spectroscopy, and molecular simulations. *J. Phys. Chem. C* **111**, 3109–3115 (2007).
- Amin, M. A. & Ibrahim, M. M. Corrosion and corrosion control of mild steel in concentrated H_2SO_4 solutions by a newly synthesized glycine derivative. *Corros. Sci.* **53**, 873–885 (2011).
- Chong, A. L., Mardel, J. I., MacFarlane, D. R., Forsyth, M. & Somers, A. E. Synergistic Corrosion inhibition of mild steel in aqueous chloride solutions by an imidazolium carboxylate salt. *ACS Sustainable Chem. Eng.* **4**, 1746–1755 (2016).
- Al-Sabagh, A. M. *et al.* Novel cationic surfactants from fatty acids and their corrosion inhibition efficiency for carbon steel pipelines in 1 M HCl. *Egyptian Journal of Petroleum*. **20**, 47–57 (2011).
- Hegazy, M. A. novel Schiff base-based cationic gemini surfactants: synthesis and effect on corrosion inhibition of carbon steel in hydrochloric acid solution. *Corros. Sci.* **51**, 2610–2618 (2009).
- Migahed, M. A., Azzam, E. M. S. & Al-Sabagh, A. M. Corrosion inhibition of mild steel in 1 M sulfuric acid solution using anionic surfactant. *Mater. Chem. Phys.* **85**, 273–279 (2004).
- Javadian, S., Yousefi, A. & Neshati, J. Synergistic effect of mixed cationic and anionic surfactants on the corrosion inhibitor behavior of mild steel in 3.5% NaCl. *Appl. Surf. Sci.* **285**, 674–681 (2013).
- Farag, A. A. & Noor El-Din, M. R. The adsorption and corrosion inhibition of some non-ionic surfactants on API X65 steel surface in hydrochloric acid. *Corros. Sci.* **64**, 174–183 (2012).
- Hegazy, M. A., El-Tabei, A. S., Bedair, A. H. & Sadeq, M. A. An investigation of three novel nonionic surfactants as corrosion inhibitor for carbon steel in 0.5 M H_2SO_4 . *Corros. Sci.* **54**, 219–230 (2012).
- Ramji, K., Cairns, D. R. & Rajeswari, S. Synergistic inhibition effect of 2-mercaptobenzothiazole and Tween-80 on the corrosion of brass in NaCl solution. *Appl. Surf. Sci.* **254**, 4483–4493 (2008).
- Wang, W. & Free, M. L., Prediction and measurement of corrosion inhibition of mild steel using nonionic surfactants in chloride media. *Corros. Sci.* **46**, 2601–2611 (2004).
- Zana, H. R. Dimeric and oligomeric surfactants. Behavior at interfaces and in aqueous solution: a review. *Adv. Colloid Interface Sci.* **97**, 205–253 (2002).
- Menger, J. F. M. & Littau, C. A. Gemini-surfactants: synthesis and properties. *J. Am. Chem. Soc.* **113**, 1451–1452 (1991).
- Menger, K. F. M. & Keiper, J. S. Gemini surfactants. *Angew. Chem. Int. Ed.* **39**, 1906–1920 (2000).
- Obot, I. B. & Obi-Egbedi, N. O. Adsorption properties and inhibition of mild steel in sulphuric acid solution by ketoconazole: experimental and theoretical investigation. *Corros. Sci.* **52**, 198–204 (2010).
- De Souza, F. S. & Spinelli, A. Caffeic acid as a green corrosion inhibitor for mild steel. *Corros. Sci.* **51**, 642–649 (2009).
- Lin, L. H., Lai, Y. C., Chen, K. M. & Chang, H. M. Oxyethylene chain length affects the physicochemical properties of sugar-based anionic surfactants with phosphates groups. *Colloids Surf., A* **485**, 118–124 (2015).
- Umoren, S. A. & Solomon, M. M. Effect of halide ions on the corrosion inhibition efficiency of different organic species – A review. *JIEC* **21**, 81–100 (2015).
- Javadian, S., Yousefi, A. & Neshati, J. Synergistic effect of mixed cationic and anionic surfactants on the corrosion inhibitor behavior of mild steel in 3.5% NaCl. *Appl. Surf. Sci.* **285**, 674–681 (2013).
- Mobin, M., Aslam, R., Zehra, S. & Ahmad, M. Bio-/environment-friendly cationic gemini surfactant as novel corrosion inhibitor for mild steel in 1 M HCl solution. *J. Surfactants Deterg.* **20**, 57–74 (2017).
- Oguzie, E. E., Li, Y. & Wang, F. H. Corrosion inhibition and adsorption behavior of methionine on mild steel in sulfuric acid and synergistic effect of iodide ion. *J. Colloid Interface Sci.* **310**, 90–98 (2007).
- Umoren, S. A. & Solomon, M. M. Effect of halide ions on the corrosion inhibition efficiency of different organic species – A review. *Ind. Eng. Chem. Res.* **21**, 81–100 (2015).
- Pavithra, M. K., Venkatesha, T. V., Vathsala, K. & Nayana, K. O. Synergistic effect of halide ions on improving corrosion inhibition behaviour of benzisothiazole-3-piperazine hydrochloride on mild steel in 0.5 M H_2SO_4 medium. *Corros. Sci.* **52**, 3811–3819 (2010).
- Quej-Aké, L., Contreras, A. & Aburto, J. The Effect of Non-ionic Surfactant on the Corrosion Inhibition of X52 Pipeline Steel in NaCl solutions. *Int. J. Electrochem. Sci.* **10**, 1809–1821 (2015).
- Sakai, K. *et al.* Adsorption and micellization behavior of novel gluconamide-type gemini surfactants. *J. Colloid Interface Sci.* **318**, 440–448 (2008).
- Mobin, M. & Rizvi, M. Adsorption and corrosion inhibition behavior of hydroxyethyl cellulose and synergistic surfactants additives for carbon steel in 1M HCl. *Carbohydr. Polym.* **156**, 202–214 (2017).
- Mobin, M., Zehra, S. & Aslam, R. L-Phenylalanine methyl ester hydrochloride as a green corrosion inhibitor for mild steel in hydrochloric acid solution and the effect of surfactant additive. *RSC Adv.* **6**, 5890–5902 (2016).
- Aslam, R., Mobin, M., Saman, Z., Ime, B. O. & Ebenso, E. E. N,N'-dialkylcystinegemini and monomeric N-Alkyl cysteine surfactants as corrosion inhibitors on mild steel corrosion in 1 M HCl solution: a comparative study. *ACS Omega* **2**, 5691–5707 (2017).
- Frisch, M., *et al* 01; Gaussian, Inc, Wallingford CT. (2009).
- Becke, A. D. Density-functional exchange-energy approximation with correct asymptotic behavior. *Phys. Rev. A.* **38**, 3098–3100 (1988).
- Lee, C., Yang, W. & Parr, R. G. Development of the Colle-Salvetti correlation-energy formula into a functional of the electron density. *Phys. Rev. B.* **37**, 785–789 (1988).

32. Miertuș, S., Scrocco, E. & Tomasi, J. Electrostatic interaction of a solute with a continuum. A direct utilization of AB initio molecular potentials for the prevision of solvent effects. *Chem. Phys.* **55**, 117–129 (1981).
33. Liu, X., Okafor, P. C. & Zheng, Y. G. The inhibition of CO₂ corrosion of N80 mild steel in single liquid phase and liquid/particle two-phase flow by aminoethylimidazoline derivatives. *Corros. Sci.* **51**, 744–751 (2009).
34. Materials Studio, Revision 6.0, Accelrys Inc., San Diego, USA, (2013).
35. Lgaz, H. *et al.* Correlated experimental and theoretical study on inhibition behavior of novel quinoline derivatives for the corrosion of mild steel in hydrochloric acid solution. *J. Mol. Liq.* **244**, 154–168 (2017).
36. Lgaz, H. *et al.* Insights into corrosion inhibition behavior of three chalcone derivatives for mild steel in hydrochloric acid solution. *J. Mol. Liq.* **238**, 71–83 (2017).
37. Sun, H. COMPASS: an ab initio force-field optimized for condensed-phase applications overview with details on alkane and benzene compounds. *J. Phys. Chem. B.* **102**, 7338–7364 (1998).
38. Saha, S. K., Dutta, A., Ghosh, P., Sukul, D. & Banerjee, P. Novel Schiff-base molecules as efficient corrosion inhibitors for mild steel surface in 1 M HCl medium: experimental and theoretical approach. *Phys. Chem. Chem. Phys.* **18**, 17898–17911 (2016).
39. Al-Sabagh, A. M., Abdul-Raouf, M. E. & Abdel-Raheem, R. Surface activity and light scattering investigation for some novel aromatic polyester amine surfactants. *Colloids Surf., A* **251**, 167–174 (2004).
40. Migahed, M. A. *et al.* Synthesis of a new family of Schiff base nonionic surfactants and evaluation of their corrosion inhibition effect on X-65 type tubing steel in deep oil wells formation water. *Mater. Chem. Phys.* **125**, 125–135 (2011).
41. Komorek, U. & Wilk, A. Surface and micellar properties of new nonionic geminialdonamide-type surfactants. *J. Colloid Interface Sci.* **271**, 206–211 (2004).
42. Touir, R., Cenoui, M., Bakri, M., El & Ebn Touhami, M. Sodium gluconate as corrosion and scale inhibitor of ordinary steel in simulated cooling water. *Corros. Sci.* **50**, 1530–1537 (2008).
43. Dagdaga, O. *et al.* Theoretical studies of cyclophosphazene derivative as corrosion inhibitor for carbon steel in sodium chloride. *Der Pharma Chemica* **7**, 46–54 (2015).
44. Miyagishi, S., Okada, K. & Asakawa, T. Salt effect on critical micelle concentrations of nonionic surfactants, N-Acyl-N-methylglucamides (MEGA-n). *J. Colloid Interface Sci.* **238**, 91–95 (2001).
45. Malik, M. A., Hashim, M. A., Nabi, F., AL-Thabaiti, S. A. & Khan, Z. Anti-corrosion ability of surfactants: a review. *Int. J. Electrochem. Sci.* **6**, 1927–1948 (2011).
46. Ramji, K., Cairns, D. R. & Rajeswari, S. Synergistic inhibition effect of 2-mercaptobenzothiazole and Tween-80 on the corrosion of brass in NaCl solution. *Appl. Surf. Sci.* **254**, 4483–4493 (2008).
47. Hegazy, M. A., Badawi, A. M. & Abd El Rehim, S. S. Corrosion inhibition of carbon steel using novel N-(2-(2-mercaptoacetoxyl)ethyl)-N,N-dimethyl dodecan-1-aminium bromide during acid pickling. *Corros. Sci.* **69**, 110–122 (2013).
48. Aiad, M. M., El-Sukkary, A., El-Deeb, El-Awady, Y. M. & Shaban, S. M. Surface and biological activity of some prepared iminium surfactants based on schiff bases. *J. Surfact. Deterg.* **16**, 243–250 (2013).
49. Khamis, A., Saleh, M. M. & Awad, M. I. Synergistic inhibitor effect of cetylpyridinium chloride and other halides on the corrosion of mild steel in 0.5 M H₂SO₄. *Corr. Sci.* **66**, 343–349 (2013).
50. Aramaki, K. & Hackerman, N. Inhibition mechanism of medium sized polymethyleneimine. *J. Electrochem Soc.* **116**, 568–574 (1969).
51. He, X. *et al.* Inhibition properties and adsorption behavior of imidazole and 2-phenyl-2-imidazoline on AA5052 in 1.0 M HCl solution. *Corros. Sci.* **83**, 124–136 (2014).
52. Mobin, M., Aslam, R. & Aslam, J. Non toxic biodegradable cationic gemini surfactants as novel corrosion inhibitor for mild steel in hydrochloric acid medium and synergistic effect of sodium salicylate: experimental and theoretical approach. *Mater. Chem. Phys.* **191**, 151–167 (2017).
53. Mu., G. & Li, X. Inhibition of cold rolled steel corrosion by Tween-20 in sulfuric acid: Weight loss, electrochemical and AFM approaches. *J. Colloid Interface Sci.* **289**, 184–192 (2005).
54. Ferreira, E. S., Giacomelli, C., Giacomelli, F. C. & Spinelli, A. Evaluation of the inhibitor effect of L-ascorbic acid on the corrosion of mild steel. *Mater. Chem. Phys.* **83**, 129–134 (2004).
55. Li, W., He, Q., Pei, C. & Hou, B. Experimental and theoretical investigation of the adsorption behaviour of new triazole derivatives as inhibitors for mild steel corrosion in acid media. *Electrochim. Acta* **52**, 6386–6394 (2007).
56. Golestani, G., Shahidi, M. & Ghazanfari, D. Electrochemical evaluation of antibacterial drugs as environment-friendly inhibitors for corrosion of carbon steel in HCl solution. *Appl. Surf. Sci.* **308**, 347–362 (2014).
57. Obot, I. B., Ebenso, E. E. & Kabanda, M. M. Metronidazole as environmentally safe corrosion inhibitor for mild steel in 0.5 M HCl: Experimental and theoretical investigation. *J. Environ. Chem. Eng.* **1**, 431–439 (2013).
58. Solomon, M. M., Gerengi, H. & Umoren, S. A. Carboxymethyl cellulose/silver nanoparticles composite: synthesis, characterization and application as a benign corrosion inhibitor for st37 steel in 15% H₂SO₄ medium. *ACS Appl. Mater. Interfaces.* **9**, 6376–6389 (2017).
59. Ma, X., Jiang, X., Xia, S., Shan, M., Li, X., Yu, L. & Tang, Q. New corrosion inhibitor acrylamide methyl ether for mild steel in 1 M HCl. *Appl. Surf. Sci.* **371**, 248–257 (2016).
60. Gerengi, H., Mielniczek, M., Gece, G. & Solomon, M. M. Experimental and quantum chemical evaluation of 8-Hydroxyquinoline as a corrosion inhibitor for copper in 0.1 M HCl. *Ind. Eng. Chem. Res.* **55**, 9614–9624 (2016).
61. Oguzie, E. E., Li, Y. & Wang, F. H. Effect of 2-amino-3-mercaptopropanoic acid (cysteine) on the corrosion behaviour of low carbon steel in sulphuric acid. *Electrochim. Acta.* **53**, 909–914 (2007).
62. Khaled, K. The inhibition of benzimidazole derivatives on corrosion of iron in 1 M HCl solutions. *Electrochim. Acta* **48**, 2493–2503 (2003).
63. Banerjee, S., Srivastava, V. & Singh, M. M. Chemically modified natural polysaccharide as green corrosion inhibitor for mild steel in acidic medium. *Corros. Sci.* **59**, 35–41 (2012).
64. Bhandari, H., Choudhary, V. & Dhawan, S. K. Influence of self-doped poly(aniline-co-4-amino-3-hydroxy-naphthalene-1-sulfonic acid) on corrosion inhibition behaviour of iron in acidic medium. *Synth. Met.* **161**, 753–762 (2011).
65. Bommersbach, P., Dumont, C. A. & Millet, J. P. Hydrodynamic effect on the behaviour of a corrosion inhibitor film: characterization by electrochemical impedance spectroscopy. *Electrochim. Acta* **51**, 4011–4018 (2006).
66. Espinoza-Vazquez, A. *et al.* Electrochemical assessment of phenol and triazoles derived from phenol (BPT) on API 5L X52 steel immersed in 1 M HCl. *RSC Adv.* **6**, 72885–72896 (2016).
67. Finsgar, M., Lesar, A., Kokalj, A. & Milosev, I. A comparative electrochemical and quantumchemical calculation study of BTAH and BTAOH as copper corrosion inhibitors in near neutral chloride solution. *Electrochim. Acta.* **53**, 8287–8297 (2008).
68. Gece, G. The use of quantum chemical methods in corrosion inhibitor studies. *Corros. Sci.* **50**, 2981–2992 (2008).
69. Sayýn, K. & Karakas, D. Quantum chemical studies on the some inorganic corrosion inhibitors. *Corros. Sci.* **77**, 37–45 (2013).
70. Solmaz, R., Kardas, G., Yazici, B. & Erbil, M. Adsorption and corrosion inhibitive properties of 2-amino-5-mercapto-1,3,4-thiadiazole on mild steel in hydrochloric acid media. *Colloids Surf., A* **312**, 7–17 (2008).
71. Kokalj, A. On the HSAB based estimate of charge transfer between adsorbates and metal surfaces. *Chem. Phys.* **393**, 1–12 (2012).
72. Lgaz, H., Salghi, R., Jodeh, S. & Hammouti, B. Effect of clozapine on inhibition of mild steel corrosion in 1.0 M HCl medium. *J. Mol. Liq.* **225**, 271–280 (2017).

73. Obot, I. B., Macdonald, D. D. & Gasem, Z. M. Density Functional Theory (DFT) as a powerful tool for designing new organic corrosion inhibitors. Part 1: An overview. *Corros. Sci.*, <https://doi.org/10.1016/j.corsci.2015.01.037> (2015).
74. Salarvand, Z., Amirnasr, M., Talebian, M., Raeissi, K. & Meghdadi, S. Enhanced corrosion resistance of mild steel in 1 M HCl solution by trace amount of 2-phenyl-benzothiazole derivatives: Experimental, quantum chemical calculations and molecular dynamics (MD) simulation studies. *Corros. Sci.* **114**, 133–145, <https://doi.org/10.1016/j.corsci.2016.11.002> (2017).
75. Kokalj, A. Comments on the “Reply to comments on the paper ‘On the nature of inhibition performance of imidazole on iron surface’” by JO Mendes and AB Rocha. *Corros. Sci.* **70**, 294–297 (2013).

Acknowledgements

Ruby Aslam gratefully acknowledges University Grant Commission, New Delhi, India for Maulana Azad National (MAN) Fellowship. The authors feel privileged to acknowledge Aligarh Muslim University Sophisticated Instruments Facility for SEM/EDAX.

Author Contributions

M.M. conceptualized and designed the work and was part of the manuscript write-up. R.A. evaluated the inhibition performance using weight loss measurements, electrochemical measurements, and surface characterization. R.A. and J.A. carried out the quantum chemical calculations. J.A. prepared part of characterization. Hassane Lgaz did M.D. simulation. All authors reviewed the manuscript and have agreed to its publication.

Additional Information

Supplementary information accompanies this paper at <https://doi.org/10.1038/s41598-018-21175-6>.

Competing Interests: The authors declare no competing interests.

Publisher's note: Springer Nature remains neutral with regard to jurisdictional claims in published maps and institutional affiliations.



Open Access This article is licensed under a Creative Commons Attribution 4.0 International License, which permits use, sharing, adaptation, distribution and reproduction in any medium or format, as long as you give appropriate credit to the original author(s) and the source, provide a link to the Creative Commons license, and indicate if changes were made. The images or other third party material in this article are included in the article's Creative Commons license, unless indicated otherwise in a credit line to the material. If material is not included in the article's Creative Commons license and your intended use is not permitted by statutory regulation or exceeds the permitted use, you will need to obtain permission directly from the copyright holder. To view a copy of this license, visit <http://creativecommons.org/licenses/by/4.0/>.

© The Author(s) 2018